Jürgen P. Böck

Controlling an artificial hand via a non-invasive BCI-system with motor imagery

MASTER'S THESIS

to achieve the university degree of

Diplom-Ingenieur

Master's degree programme: Biomedical Engineering

submitted to

Graz University of Technology

Supervisor

Univ.-Prof. Dipl.-Ing. Dr. techn. Gernot R. Müller-Putz

Institute of Neural Engineering

Graz, August 2016

AFFIDAVIT

I declare that I have authored this thesis independently, that I have not used other than the declared sources/resources, and that I have explicitly indicated all material which has been quoted either literally or by content from the sources used. The text document uploaded to TUGRAZonline is identical to the present master‘s thesis.

Date

Signature

Acknowledgments

I would like to use this chance, to thank Prof. Gernot Müller-Putz for the interesting and challenging topic I could work on.

I want to thank the staff from the “Institute of Neural Engineering” for their patience in answering my questions.

Finally, all my friends’ help is appreciated.

Thank you very much!

Abstract

Brain-Computer Interfaces are systems which are used to transform the user's brain activity to signals which are used to solve a given task. Motor imagery is one of these activities which can bring back the ability to a user to control the outer world with the EEG signals measured at the user's scalp.

The aim of this thesis is to investigate the corresponding signals and areas on the cortex which are produced during motor imagery while flexing and extending the fingers and pronating and supinating the hand. Therefore, an artificial hand was built to simulate the correct classification to the subjects.

EEG-data of eight able-bodied subjects were recorded while performing motor imagery of the two class problem. The two classes were the motor imagery of the two previously described movements of the fingers and the hand. The neuroanatomy suggested that these signals should be higher in the area of the motor cortex of the ipsilateral side of the hemisphere. Another area which should be activated during motor observations is the Brodmann area 44. The results show that in the frequency band between 8 and 40 Hz a low classification accuracy is achievable. This was caused by the narrow areas which are activated or deactivated during the emerge of the two movements on the cortex. As the subjects attending this experiments were naive BCI users these areas were small. Therefore, it is highly suggested to train the participants multiple times to get more neurons involved and to enlarge the areas. The concentration of the subjects and the motivation has to be guaranteed to be high during the tasks because otherwise the results are not optimal.

KEYWORDS: cue-based BCI, motor imagery, EEG, Prosthesis, Dextrus Robotic Hand

Kurzfassung

Die Gehirn-Computer Schnittstellen stellen Systeme dar, welche die Gehirnaktivitäten eines Nutzers in Signale transformieren, um eine definierte Aufgabe zu lösen. Die Bewegungsvorstellung ist eine dieser Aktivitäten, welche dem Benutzer die Möglichkeit zur Kommunikation mit der Außenwelt zurückgeben kann. Dies geschieht mit den am Kopf des Benutzers gemessenen EEG-Signalen.

Ziel dieser Arbeit ist es, die Signale und Areale am Cortex zu untersuchen, welche für die Bewegungsvorstellung zum Beugen und Strecken der Finger und für Drehbewegungen der Hand im Unterarm verantwortlich sind. Die dafür fertiggestellte künstliche Hand soll den Testpersonen die korrekte Klassifikation simulieren.

Die EEG-Daten von acht gesunden Probanden wurden während der Bewegungsvorstellung eines zwei-Klassen-Problems aufgenommen. Die beiden Klassen waren die Bewegungsvorstellung der beiden bereits beschriebenen Bewegungen der Finger und der Hand. Die Literatur der Neuroanatomie lässt darauf schließen, dass die Amplituden der Signale auf der ipsilateralen Seite der Hemisphäre im Bereich des Motorcortexes prominenter sind. Das Brodmann Areal 44 sollte bei beobachteter Bewegung ebenfalls aktiviert sein. Die Resultate zeigen, dass für ein Frequenzband zwischen 8 und 40 Hz eine niedrige Klassifikationsgenauigkeit erreicht werden kann. Die örtliche Nähe der aktivierten beziehungsweise deaktivierten Areale am Kortex für die beiden Bewegungen sind ein Grund für dieses Ergebnis. Die Teilnehmer für dieses Experiment hatten keine Erfahrung mit BCI-Systemen und die Areale am Cortex waren durch das fehlende Training klein. Daher wird dringend empfohlen, die Teilnehmer mehrmals mit dem BCI-System zu trainieren und dadurch mehr Neuronen zu involvieren und die Areale zu vergrößern. Es ist sicherzustellen, dass die Konzentration und die Motivation der Probanden während der Aufgaben hoch sind, um optimale Ergebnisse zu erhalten.

SCHLÜSSELWÖRTER: synchrone Gehirn-Computer Schnittstelle, Bewegungsvorstellung, EEG, Prothese, Dextrus Roboterhand

Table of Contents

Abbreviations

BCI	…	Brain-Computer Interface
CAR	…	Common Average Reference
CSP	…	Common Spatial Pattern
EEG	…	Electroencephalography
EMG	…	Electromyography
EMI	…	Electromagnetic Interference
EOG	…	Electrooculography
ERD	…	Event-Related Desynchronization
ERS	…	Event-Related Synchronization
FDM	…	Fused Deposition Modelling
FES	…	Functional Electrical Stimulation
LDA	…	Linear Discriminant Analysis
Lig.	…	Ligament
Ligg.	…	Ligaments
M.	…	Muscle
MM.	….	Muscles
Ncl.	…	Nucleus
PCB	…	Printed Circuit Board
PWM	…	Pulse-Width Modulation
SNR	…	Signal to Noise Ratio
SVM	…	Support Vector Machine

1 Introduction

When the EEG signals were measured for the first time, nobody could imagine that the derived information could for example be used for controlling artificial limbs. Back in 1929, Dr. Berger published a paper, describing the first EEG frequency bands [1]. Dr. Grey Walter visited the laboratory of Dr. Berger and improved the machinery to measure EEG. In 1964 Dr. Grey invented the first Brain-computer interface [2]. Once computer got smaller, more capable and available for more people it was a reasonable step to build systems, which interact with the person's thoughts. In this area, Hollywood was not as fast as it used to be by technical things in movies, which are impossible for science during the shoot. One example is Gene Rodenberry's series episode of 1966 [2]. But since then, movies have shown BCI-systems, which are able to do things engineers are dreaming of for centuries. Nobody would deny that these movies could be a treasure chest for more inventions to come by simply being influenced by them. The ability to replace a limb or even a hand when necessary or compensate the loss of one is something, which returns a person an ability that can make life easier. Letting artificial devices interact with EEG is the even-handed step forward to make this happen. The field of research is growing and scientists of many different areas are working on systems to make everybody's life easier. [3]

1.1 Aim of this Thesis

In this thesis an EEG driven artificial hand is built. For the EEG part, a two class BCI is developed. One class is flexing/extending the right hand's fingers and the other one is turning the right forehand for pronation and supination. Paek et al. published in 2014, that it was possible to decode the movement of the index finger of the EEG. For that reason, the finger tapping of the index finger was recorded with a data glove and the EEG was measured [4]. Liao et al. (2014) could demonstrate that the findings derived by electrocorticography (ECoG) could be useful for detecting finger movements of the whole hand [5]. Yong et al. (2105) investigated the possibility to decode different imagery movements of the same limb [6]. Although the accuracies are not very high, it was shown that it is possible to build a BCI-System and control a neuroprostheses with unintentional left/right hand or food imagery [7], [8]. The goal of this thesis is to build a hand prosthesis which is controlled by actually thinking on the corresponding movement. Therefore, the imagery movement of all fingers and the wrist (supination

or pronation of the hand) shall be recorded and being used to move the Dextrus' fingers and the thumb. In this thesis, the thumb demonstrates the correct classification of the imagery movement of the wrist, because the artificial hand is not able to perform a supination or pronation. As the areas on the brain responsible for this actions implies, this is a difficult aim. According to the findings of previous studies, there might be an activation to detect in the area 44 of Brodmann during the observation of the moving hand [9]. As reported, the sensorimotor areas should be among the brain's activated regions during these tasks [10].

1.2 Theoretical Background

In this chapter the theoretical background for the further chapters is given. The first part deals with the anatomy of the human hand and is followed by the neuroanatomy. After that the electroencephalogram and the brain-computer interface are described and a short explanation of the open-hand-project is given.

1.2.1 Anatomy of the Human Hand [11]

The hand's structure is linked to the grasp-functionality. This is mainly achieved by separating the thumb [*pollex*] from the four other fingers. Therefore, it is possible to oppose the thumb. The palm of the hand [*palma manus*] is necessary to rest the things, which were grasped. This implies the necessity of a three-structured hand: *Carpus, Metacarpus, Phalanges*. The same goes with the skeleton differences between the first digit of the hand and the others. The wrist bones [*carpals*] are arranged in two rows. The proximal row is constituted of three, the distal row of four bones. The bones are fit into each other to form the *palma manus*. The ligament *Retinaculum flexorum* goes from the *Eminentia carpi ulnaris* to the *Emanentia carpi radialis*. This canal is called *Canalis carpi* and is useful to guide the tendons of the hand. The whole distal and proximal carpi are moveable against each other [*Articulatio mediocarpalis*] and summed up they are moveable against the forearm [*Antebrachium*]. Except for the saddle joint, the joints of the metacarpale bones are fixed by obliquely going ligaments [*Ligg. Metacapalia dorsalia and palmaria*] and build an amphiathrosis [*Articulationes carpometaarpales*]. Ligaments stabilise the cove of the hand.

Because of its two degrees of freedom and two axes the saddle joint acts as a spheroidal joint. Whereas the metacarpophalangeal joints [*Artiulationes metacarpophalangae*] are spheroidal joints too but the ligaments prevent some movements.

The joints between the metacarpal bones and the phalanges of fingers II too V [*Articulationes metacarpophalangeales II–V*] are spheroidal joints [*Articulatio speroidea*]. Ligaments tighten these

joints which results to seem that these have two degrees of freedom. A third degree, rotating the finger orthogonal to the flexion or extending axis, can only be performed manually.

The knuckle joints [*Articulationes interphalangeae manus*] are hinge joints. There are guide bars in the sockets of the joints. This gives them one degree of freedom.

1.2.2 Neuroanatomy

The brain [*encephalon*] is connected via the spinal cord to the entire body. The encephalon, as shown in Figure 1, consists of the medulla oblongata, pons, mesencephalon, diencephalon, cerebellum, and telencephalon.

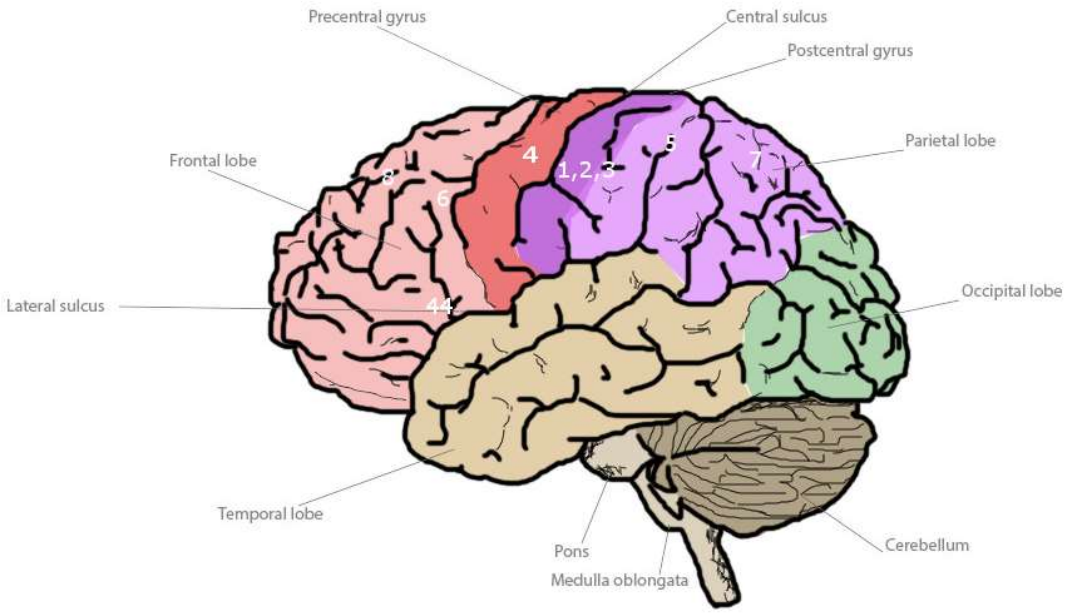

Figure 1: The brain and its areas and Brodmann areas 1, 2, 3, 4, 5, 6, 7, 8 and 44

The transverse section of the spinal cord shows grey and white matter. In the axial section the grey matter is butterfly-shaped and contains the perikarya of the spinal cord's neurons. The anterior part is called cornu anterius and contains motoric neurons whereas the cornu posterius contains the sensory neurons. The cornu laterale contains primarily neurons of the autonomic nervous system. All sections together form the different columns of the spinal cord. The cross-section can also be subdivided into ten laminae (I – X) according to Rexed. This is similar to Brodmann areas of the brain, which are assigned to certain areas on the brain's cortex and shown by a defined number. [12]

The Radix anterior or radix posterior exits or enters the spinal cord. The cells in the laminae VIII and IX and therefore in the cornu anterius are responsible for the muscles in the periphery. These are mainly the so-called α-motor neurons and are big multipolar neurons. In the cornu anterior the smaller β- and

γ-motor neurons can be found too. The γ-motor neurons are responsible for exciting the muscle spindle, thus to magnify the response on stretch stimuli. This is necessary to fine tune the movements. The cells of the laminae I to VII are in the cornu posterius. Here the fibres are found which carry the sensible impulses such as pain, and proprioception (a sense of the position and movements of body parts). [12]

The fibres of the pyramidal tract [tractus corticospinalis], which already crossed sides in the medulla, go on as the *tractus corticospinalis lateralis* in the lateral funiculus of the spinal cord either to interneurons or to motor neurons of the *cornu ventrale*. 10-30% of the fibres of the pyramidal tract go on as tractus corticospinalis anterior and cross to the other side in the segmental levels.

The *tractus spinocerebellares posterior et anterior* have their origins in the *Pars sacralis*, *thoracalis* and *lumbalis medullae*. Here the impulses of the lower limbs are propagated. The *tractus spinocerebellaris superior* is the functional equivalent for the upper limbs.

In the mesencephalon the substantia nigra is part of the areas of the brain which are responsible for modulation and control of movement sequences. The substantia nigra receives afferents mainly from the striatum and from the cortex of the telencephalon. The afferents received by the telencephalon are mainly coming from the motoric cortex and from the premotoric cortex.

The *crura cerebri* is made of the *fibrae corciconucleares* among others which contains motoric fibers of the contralateral side.

In the cerebellum the pontocerebellum if found which is responsible for the fine-tuning of the motion sequences, which are generated by the motoric cortex.

The thalamus, a structure of the diencephalon, is important for the coordination of the locomotor system.

For this thesis the structure in the border between the frontal and parietal lobe is of interest. The motoric cortex is found on the side of the frontal lobe; the sensible cortex on the parietal lobe of the telencephalon

The surface of the brain is built by ridges and furrows. These ridges, the so-called gyri and the furrows, the so-called sulci increase the surface area.

The frontal lobe is mainly formed by the gyrus frontalis superior, gyrus frontalis medius, and gyrus frontalis inferior. These gyri are separated by the sulcus frontalis superior and the sulcus frontalis inferior. The gyrus frontalis inferior can be subdivided into the pars orbitalis, pars triangularis, and pars

operularis. These structures edge the sulcus lateralis. The motoric cortex is found in front of the sulcus centralis and is known as gyrus precentralis.

The gyrus precentralis represents the Brodmann area 4. (Brodmann, a german anatomist, originally defined 52 areas.) [13]

The gyrus precentralis is the final progression of steps galore creating movement. Along the gyrus it is possible to draw a representation of the body. This is the so-called motoric Homunculus. The size of the area which corresponds to a body part is different. The finer the muscle-functions the bigger the area. The hands and the mouth region are represented by a relative big area, as seen in Figure 2. [11]

The representation of the human body on the cortex is shown in Figure 3.

Figure 2: Homunculus: Representation of body parts in respect to the actual size on the cortex

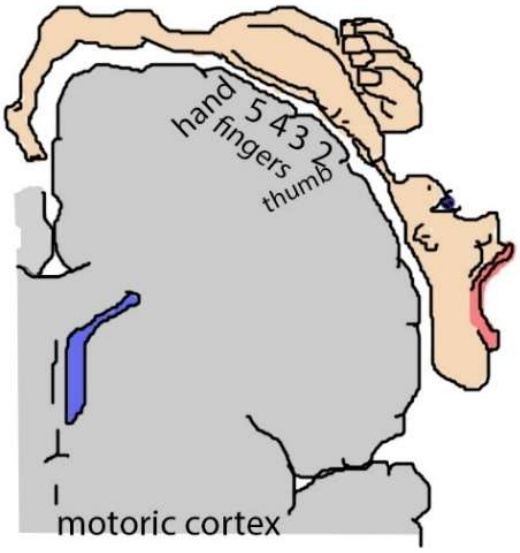

Figure 3: Representation of the Homunculus on the motoric cortex

The premotoric cortex is important for preparation for locomotion. It is located in the Brodmann area 6. The organisation is not as precise as the one of the motoric cortex. It is responsible for movements which are activated by tactile (area 5) or multimodal sensory (area 7) information. Complex movements are planned in Brodmann area 8. The other parts of the premotoric cortex influence the planning of movements and are therefore important for the initiation of movements. [11]

The striatum and pallidum are the nuclei inside the telencephalon. Both are part of the locomotor system (see Figure 4). The striatum inhibits the pallidum and the substantia nigra. This gives the striatum the possibility to inhibit or promote motoric impulses. The same does the pallidum with the thalamus. How the different structures of the brain influence each other is shown in Figure 4.

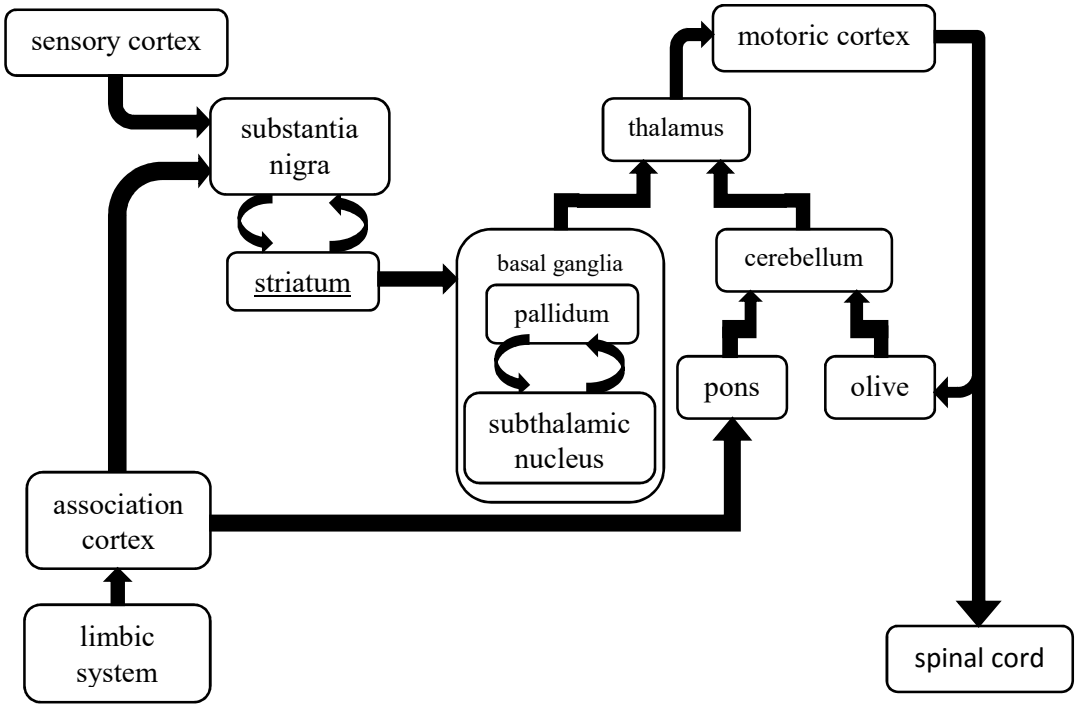

Figure 4: Schematic of the structures in the brain for designing and executing motoric impulses

1.2.2.1 Innervation of the human hand

In the previous sections the pathway through the central nervous system was discussed. This section gives an overview on how the different muscles of the hand can be operated. The human hand consists of several muscles as can be seen in Figure 15 and Figure 17 displaying muscles and tendons of a right hand viewed from dorsal. It would not be very useful if all of them were controlled by one nerve. Therefore, multiple nerves are controlling different parts of the hand, exciting and approaching the spinal cord at C5 to C8. The evolution came up with the nerves and muscles as shown in Table 1. In this thesis not only the movement of the human hand itself is of interest, however, also the muscles for pronation and supination are under investigation as well. The pronation – which is the inside-rotation of the hand - is mainly performed by two muscles: *m. pronator teres* and *m. pronator quadratus* and are innervated by the median nerve. The counter movement is done by the m. supinator and the *m. biceps brachii*. The latter gets its nervous signals from the *nervus musculocutaneous* whereas the supinator is innervated by the deep branch of the radial nerve.

Table 1: Innervation of the hand's muscles

Nerve	Innervation by the nerve
Radial nerve	Extensor carpi radialis longus muscle Extensor carpi radialis brevis muscle Extensor carpi ulnaris muscle Extensor digitorum muscle Extensor digiti minimi muscle Extensor pollicis longus muscle Extensor pollicis brevis muscle Abductor pollicis longus muscle
Medial nerve	Flexor carpi radialis muscle Flexor pollicies longus muscle Flexor digitorum superficialis muscle Flexor digitorum profundus muscle Palmaris longus muscle Opponens pollicis muscle Abductor pollicis brevis muscle Flexor pollicis brevis muscle (caput superficialis) 1st and 2nd Lumbricals
Ulnar nerve	Flexor carpi ulnaris muscle Flexor digitorum profundus muscle Opponens digiti minimi muscle Flexor ditgiti minimi brevis muscle Abductor digiti minimi muscle Dosal interossei muscles Palmar interossei muscles Adductor pollicis muscle Flexor pollicis brevis (Caput profundus). 3rd and 4th Lumbricals

1.2.3 Electroencephalogram

In 1929, Professor Dr. Hans Berger published the first signals recorded on a human scalp in "Über das Elektrenkephalogram des Menschen". As these signals are measured non-invasively, they are measured more or less easily. In the following years, more articles were added under the same title. He called his findings electroencephalogram, shortly known as EEG [1]. Later studies revealed more about the "brain waves".

Almost thirty years later the internationally standardized 10-20 system developed by the Canadian neuroscientist Herbert Jasper brought the feasibility to compare and reproduce the findings of other

researchers more easily [14]. Till today, more standardized systems are in use: like the equidistant system and caps with smaller distances between the electrode positions.

Another big step was made when computer became smaller and more powerful. Now it was possible to get to the next step: connect computer and humans. This was the birth of the brain-computer interface (BCI). The non-stationary nature of EEG signals was one major problem. Hormones, as well as the personal condition on a particular day and time influence the EEG. This means that the adjustment has to be done regularly and for every experiment. These continuous tunings are the basis of a good brain-computer interface system.

Nevertheless, how shall the computer be fed with the information? As there are always different noise sources and other signals which overlay the EEG, it is obvious that the data has to be filtered and pre-processed. After that there has to be a way for interpretation of the data. There are various ways to do this. One way is to think of the EEG as a stochastic signal. Another approach is to look at it deterministically. Either way it is not the "real" EEG. There are unalike noises and the insufficient reduction of the noises as well as several neurons producing the electric field and therefor the measured amplitude of some microvolts and the lack of direct correlation with single neurons which alter the EEG.

Artefacts, such as EMG and EOG can be measured and algorithms can reduce the influences of these signal on the EEG data. Nevertheless, the noises will always interact with the original EEG in a way that makes it impossible to get pure EEG and to extract the different frequency bands easily. The hair, skin, skull, and the liquor form a distance between the arising signals of the nerve cells in the cortex and the electrodes. These factors cannot be withdrawn without being invasive. The non-invasive approach's goal is that during measurement the noise sources are reduced as good as possible for example by applying gel on the electrodes and putting the hair away, which means to increase the SNR. The area for the hand is like previously mentioned in the Brodmann area 6. Despite the fact that the motoric cortex is the last step for the formation of a movement, it is the only way to measure something related to it via EEG. A schematic of the cortex and the corresponding body parts is shown in Figure 3.

1.2.3.1 Frequency bands

Well known components of the EEG are the following frequency bands: The delta, theta, alpha, beta and gamma oscillations.

The delta waves are in a range below 4 Hz and are associated with coma. The theta waves are defined with a frequency between 4 and 8 Hz and can be seen during specific sleep states, mediation and drowsiness. Relaxation and readiness is marked by the alpha rhythm in the range of 8 to 13 Hz.

Frequencies between 13 and 25 Hz are called beta rhythm and are associated with active concentration, anxiety and focused attention. Frequencies above 25 Hz up to 200 Hz are called the gamma frequency band, which occur during peak performance and arousal. [15]

1.2.3.2 Event-related synchronization / desynchronization

Like the terms imply, there is a desynchronization (power decrease) shown during an event and afterwards a synchronization (power increase) takes place when the deactivation of the cortical area occurs. [16] This information is derived by calculating the relative power in a certain frequency band and interval in respect to a reference interval. By definition the ERD is shown in red and ERS in blue colour.

The sensorimotor rhythms can be subdivided in mu rhythms and beta rhythms. The frequency range between 8 and 10 Hz is called low mu rhythm, between 10-12Hz high mu rhythm. This frequency band may vary from subject to subject. Subsequently the beta band reaches up to 30Hz. The power of the mu and beta rhythm is changed by motor imagery and results in ERD/ERS. With the help of these it is possible to distinguish the body parts. [17]

During active muscle activation and therefor moving for example the limb and even during imagining the movement, these changes are recognizable. To visualize these closely bounded effects, a time-frequency map is used. The phenomenon is weaker during imagery motor execution compared to the active movement. As known, the contralateral hemisphere is responsible for movements of the other side of the body and the ERD/S is more prominent on this side of the brain. Nevertheless, on the ipsilateral hemisphere these changes in power are visible too, but are commonly less pronounced. [18]

1.2.3.3 Spatial and temporal resolution of EEG

The spatial resolution of EEG is in the dimension of some millimetres and the temporal resolution is in the range of milliseconds. [19]

1.2.4 Brain-computer interface

The brain-computer interface is the connection between the human brain and the outer world through the use of a computer. In this case the EEG signals and its frequency bands are interpreted and classified. With the received information different tasks shall be solved. For instance, in this thesis the artificial hand shall perform the movements the person wants it to. Although it might seem straightforward, it is not. On the one hand, as mentioned before, there are artefacts which worsen the measured EEG-signal. On the other hand, there is the complexity of the brain, the anatomy of the head, and the human itself. The anatomy and physiology is slightly different for each individual and even the standardised systems cannot overcome these pitfalls completely. The compliance of the person is

another factor which has to be taken into account. It is somehow depending on the person's condition whether the experiment goes well or not, because nobody can insure that the needed tasks are determined correctly. In other words: the importance and the motivation has to be kept high in the person's mind.

Apart of arising problems because of the person who is tested, there are technical difficulties too. The SNR is needed to be as high as possible. As previously mentioned, the acquiring of the EEG is done as good as possible. The pre-processing is the next step to reduce the noise and eliminate artefacts. Now the features are extracted and classified after filtering the signals. To reach this point a lot of work has to be done but then it might be possible to interact with the system in the way the instructor has wanted it since the beginning.

1.2.4.1 Cue-paced BCI

This kind of BCI systems is based on a paradigm, which is shown on a screen to the subject. The response of the subject is according to the cues presented, therefore also giving it the name of synchronous BCI. In contrast to the asynchronous BCI, the cue-paced BCI has its fixed scheme and accepts the subject's instructions only within a predefined time window starting by a cue. The advantage of a cue-paced BCI is that the EEG signals may not be affected in that extend like it is the case with the asynchronous BCI because the user can be told to avoid generating artefacts in the certain time window [20]. With these facts in mind it is decided to use a cue-paced BCI for this thesis.

1.2.4.2 Self-paced BCI

An EEG-based self-paced (asynchronous) BC system is uncued and user-driven. As this implies, the user decides when something happens and what shall be done. It is obvious that this kind of BCI system is the one which copies the natural interaction of all the coupled systems in the living body. As it was shown in previous studies by Pfurtscheller et al. (2005) [21], a motor imagery of left vs right hand and feet could be used to regain some control over a hand by functional electrical stimulation. The design is much more difficult than the cue-paced BCI and the same goes for the evaluation [20].

1.2.4.3 Feature Extraction and Selection

The measured EEG signals are hard to interpret in the first place. The EEG arousal has to be processed by the BCI system. Hence, the features of the response to the cue have to be identified. The signal features should represent the patterns of the motor imagery while other signal components are not selected for further investigations. The traditional way is to compute the frequency spectra or to analyse the signal in the time domain. The band power is one of the most used type of features. This can be done by calculating either the Fast Fourier Transform of the signal and therefor transform it from the time to the frequency domain and filtering it or by filtering the signal in the desired frequency

range and squaring it in the time domain. Hence the EEG signal is a biological signal with no fixed frequency spectrum the time and frequency analysis is used to identify characteristic signal components which represent the signal best. The time domain is used in BCIs for example for evoked potential amplitudes or neuronal firing rates whereas the frequency domain is used e.g. for mu and beta-rhythm amplitudes [22]. The time-domain features on the other hand are considered as a good choice for real-time BCI-systems [23].

The most effective way to extract the features of motor imagery EEG is the common spatial pattern (CSP) method [24]. With this procedure the difference between the signal of two classes is maximized in an offline training. The variance of one condition is maximized while the variance of the other condition is minimized.

1.2.4.3.1 Common Spatial Pattern [25]

The prior assumptions are that the frequency bands are identified and that the time frames are known. The paradigm defines this time windows. Within this time window the signal is assumed to be Gaussian. The last expectation is that the two conditions are separable. This means that the source of these two classes differ. Therefore, it can be described as an optimization problem. Let X be the raw EEG-Signal represented by an chxN matrix with ch representing the number of channels and N the number of samples in the chosen time interval (trial) t.

$$\boldsymbol{X} \in \mathbb{R}^{\boldsymbol{chxN}} \qquad (1)$$

$\boldsymbol{X}$ consists of $\boldsymbol{X_a}$ and $\boldsymbol{X_b}$ with a and b being the two classes. The spatial covariance matrix of the bandpass filtered EEG per trial is represented by

$$\sum_{\boldsymbol{t}} = \boldsymbol{X_t X_t}^{\boldsymbol{T}} \in \mathbb{R}^{\boldsymbol{chxch}} \qquad (2)$$

Whereby the covariance matrix per class c (either a or b) is a subspace of $\sum_{\boldsymbol{t}}$ and is represented by

$$\sum^{(\boldsymbol{c})} = \langle \sum_{\boldsymbol{t}} \quad \rangle^{\boldsymbol{c}} \qquad (3)$$

The spatial filter $\boldsymbol{W_c}$ is optimised for class c as

$$\boldsymbol{W_c} = \mathbf{max}_{\boldsymbol{W}} \ (\boldsymbol{W^T} \sum^{(\boldsymbol{c})} \boldsymbol{W}) \qquad (4)$$

such that spatial filtering of the average covariance matrix of both classes holds

$$\boldsymbol{W^T} (\sum^{(\boldsymbol{a})} + \sum^{(\boldsymbol{b})}) \boldsymbol{W} = \boldsymbol{I} \qquad (5)$$

With this constrain $\boldsymbol{W}$ cannot be chosen to be infinite and maximises the variance for one class and minimises the variance for the other class.

The way this is implemented in the Graz-BCI is by generalizing the Eigenvalue. After computing the spatial filter, the first columns of the spatial filter yield the largest variance for one class and the last columns the largest variance for the other class (for this thesis the first and the last three columns are chosen).

This works best when dealing with continuous BCI and two classes and this is the case for this thesis. Furthermore, CSP has a high accuracy with motor imagery. [26]

1.2.4.4 Classification

The classification process identifies the signal features and assigns them to one of the classes. Depending on the nature of these features, various classifiers are available. The main classifiers which use a linear function to distinguish the classes are the linear discriminant analysis (LDA) and the linear or non-linear support vector machine (SVM). Although there is a variety of classifiers available, among others, the quadratic discriminant analysis, artificial neural networks, independent component analysis, hidden markov models (HMM) or the second order method named principal components analysis, the LDA and SVM perform marginally worse in comparison to more complex methods [27].

State of the art in BCI-systems is the linear LDA.

1.2.4.4.1 Linear Discriminant Analysis

The LDA classifier provides high accuracy and has a low need of computational power [26]. This leads to a good tool when using online BCI. The LDA classifier for two classes works as follows: The data of two classes are considered linear separable. A plane in the feature space assigns a feature to a certain class, depending on which side of the plane the feature is found. By adding a distance to this plane, the certainty can be increased, that the feature belongs to the selected class. The vector $\vec{w}$ orthogonal to the hyperplane describes the distance and is defined such as

$$\vec{\boldsymbol{w}} \propto \left(\sum^{(\boldsymbol{a})} + \sum^{(\boldsymbol{b})}\right)^{-1} (\bar{\boldsymbol{a}} - \bar{\boldsymbol{b}}) \qquad (6)$$

where $\bar{a}$ and $\bar{b}$ are the means of each class. [28]

This means that LDA reduces the dimensionality and preserves most of the class discriminatory information.

1.2.4.5 Active Electrodes

These type of electrodes are sintered Ag/AgCl electrodes, which work in a frequency range of 0 to 100kHz. Active electrodes outperform the passive variant by reducing or avoiding artefacts and signal noise [29]. This is done by adding an additional noise pre-amplifier inside the electrodes. The montage time of the EEG-cap is short for this type of electrodes compared to the passive EEG-electrode

equipment. A gel has to be applied beneath the electrode. It is crucial that there is no shortcut built with the gel to the other electrodes.

1.2.4.6 EEG-Cap

As the spatial coverage increases with a denser system the development goes on from the first proposed standardized 10-20 system to the 10-5 system which can hold 128 channels. For this thesis 61 EEG-channels are used in an equidistant arrangement.

1.2.4.7 Surface Laplace

A famously used method within BCI-systems is Surface Laplace. The signal of the nearest neighbour electrodes is weighted and subtracted of the electrode's signal, which is surrounded by these electrodes, as described by equation 1. Laplace is the 2nd derivative [30] over space of the scalp potential in both surface directions, which means the latitude and longitude of the scalp (best fitted as spherical surface). The data is converted into a reference-free current density. The difference is built between the potential-difference of the electrode and ground and the potential-difference of the ground and reference. The weighted subtraction of the surrounding electrodes is possible as the reference electrode is automatically removed, which should be the potential common to all electrodes. Thus, the electrode has not to be at a fixed position and is not influencing the surface Laplacian estimation. It is shown that the nearest-neighbour Laplacian predicts the target position best whereby the next-nearest Laplacian produces signals for better accuracy [31].

$$\boldsymbol{E_{LAP} = E_{center} - \frac{1}{4} \sum_{i=1}^{4} E_{surrounding,i}} \qquad (7)$$

E_{LAP} is the next-nearest Laplacian (small Laplacian) computed by the difference of the centre electrode E_{center} and the weighted sum of the four surrounding electrodes $E_{surrounding}$.

The Hjorth surface Laplacian only holds for evenly spaced electrodes on an orthogonal Cartesian grid.

1.2.4.8 Common Average Reference

McFarland et al. proved that the common mode reference (CAR) and Laplacian methods provide a better signal-to-noise ratio for mu-rhythm than the standard ear-reference method does [32].

The CAR is computed according to formula 8.

$$\boldsymbol{E_{electrode,CAR} = E_{electrode} - \frac{1}{n} \sum_{i=1}^{n} E_{electrodes}} \qquad (8)$$

$E_{CAR,electrode}$ is the common average reference potential for the Electrode with the potential $E_{electrode}$ and n is the number of electrodes in the montage, whose potentials $E_{electrodes}$ are summed up. This is done for every electrode in the montage.

1.2.5 Prosthetics

The idea of replacing missing body parts has been mentioned throughout the history. Dating back to the Ancient Egyptian Empire, missing toes were already replaced by similar looking wooden prostheses. Artefacts of these kind have been found in other parts of the world since then. It is speculated whether there were hand prostheses before the Renaissance or not. [33]

The ancient prosthesis had to be adjusted and could not perform any movement without manually adjusting the moveable parts. In the recent years, prostheses have been developed which are connected with the neural system of its user and got further than the simple compensation of a limb. These so-called neuro-prostheses are not only hands or foots being replaced or controlled via EEG but also e.g. retina or cochlea implants.

In combination of a Brain-Computer Interface, these prostheses are controlled by the user in almost real-time. Persons, whose peripheral nerves are still intact and cannot control their limbs because of a disconnection in the spinal cord, may get back some of the functionality of their own limbs via functional electrical stimulation (FES) or the replacement of a limb is controlled by the BCI.

1.2.6 The open hand project

Joel Gibbard founded the open hand project as an indiegogo project in 2013. The so-called Dextrus hand is a robotic hand. It is assembled by 3D printed plastic parts, which are downloadable in STL-file-format and the finished hand can be moved via EMG with the help of cables, electric motors, and bearings.[1]

The functionality of the hand is limited to six degrees of freedom, one for every finger, and an extra degree for the thumb. The thumb consists of two joints and the other fingers of three joints. Due to this fact, the movements possible are extension and flexion of all fingers separately and opposition of the thumb. These are the main movements prosthesis are able to do.

The Dextrus robotic hand is able to accomplish two different main grasp types: The pad opposition and the palm opposition. These give the opportunity to perform some basic grasps out of the possibilities a human hand is capable of. According to Feix et al (2015) the human hand's movements can be classified into 33 unique grasps [34]. In consequence of the Dextrus hands' reduced degrees of freedom, not all of these movements are possible. The assigned intermediate types may be not available as well as most of the precision positions. The latter can be achieved by some adjustments but the lack of proper feedback by the Dextrus v1.1 robotic hand appears as a big disadvantage for this kind of tasks. The power grasps occur to be the one the designer of the artificial hand had in mind.

[1] Open Hand Project, 2013, Open Hand Project [ONLINE] Available at: http://www.openhandproject.org/ *[Accessed 5 Mai 2015]*

An advantage is the single actuation of each digit, which facilitate the pincer grip.

The Dextrus hand is going to be developed further but for this thesis the Dextrus hand version 1.1 is built and the movements shall be acted out via computing EEG signals. This attempt completes the original idea of controlling the hand with EMG by the founder of the Dextrus hand.

1.3 Outline of the Thesis

This thesis is subdivided into five main chapters.

The first chapter gives a theoretical background. It provides the anatomical facts about the human hand and the neuroanatomy. Furthermore, it introduces and explains a Brain-Computer Interface and prosthetics and it defines the aim of the thesis.

The second section “Methods” describes how the goal is reached and how the single components are assembled together to build the whole brain-computer interface. Furthermore, an overview is given about the settings of the brain-computer interface and how the interaction between the electroencephalogram and the bionic hand is solved.

Chapter 3 presents the results.

Chapter 4 discusses the findings of this thesis.

Chapter 5 summarises the findings of this thesis and gives an outlook for future improvements and further investigations.

2 Methods

2.1 The Dextrus – open hand project

The Open-Hand-Project-Website[1] provides the 3D parts in an STL-file format and a shopping list for the needed material like screws, springs and motors. These files are triangulated representation of the Dextrus robotic hand. The tensioners and the spindles are not scaled properly. Therefore, these parts are adjusted with the help of a 3D-software, that they fit into the designated spot. The result after these preliminary considerations is shown in Figure 5. Figure 5 shows the 53 individual parts needed to be printed for building the Dextrus v1.1 Robotic hand.

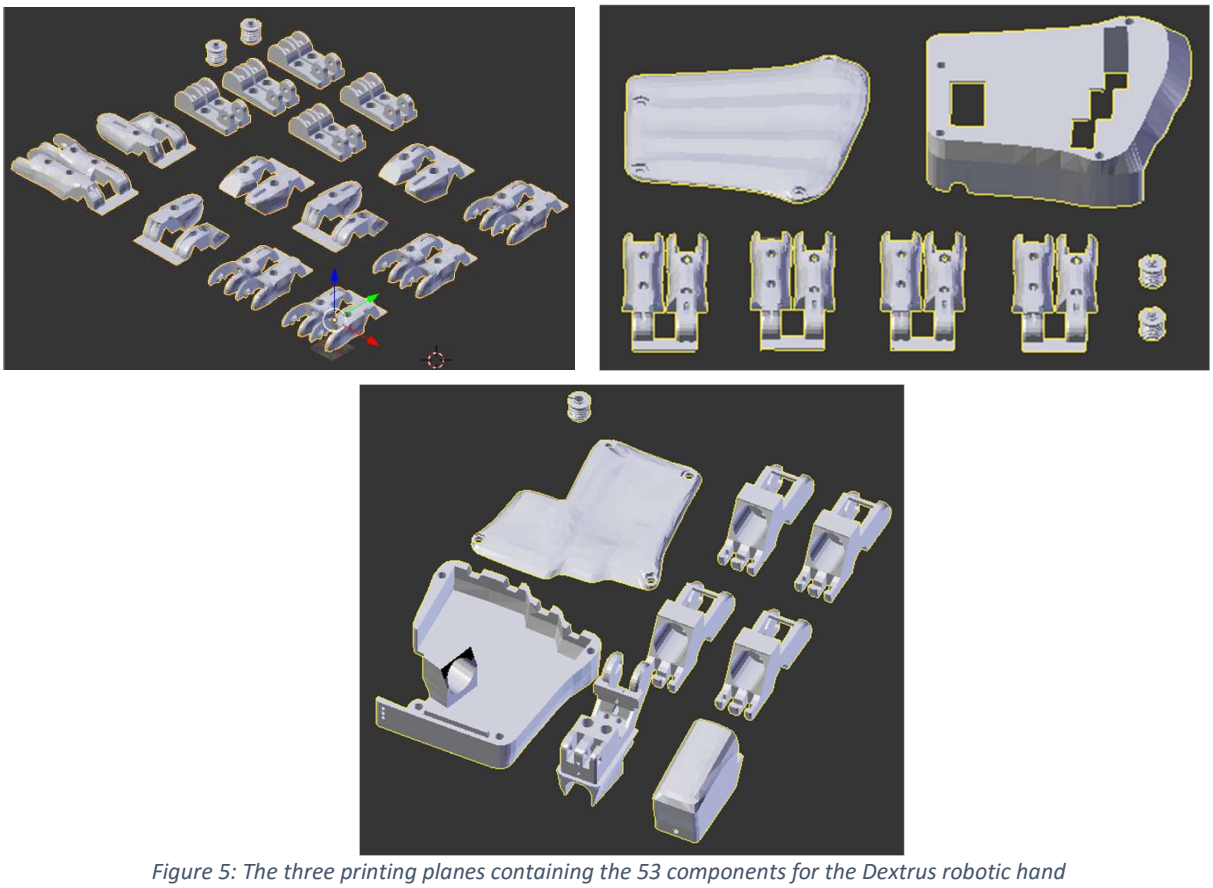

Figure 5: The three printing planes containing the 53 components for the Dextrus robotic hand

[1] Open Hand Project, 2013, Dextrus v1.1 Robotic Hand [ONLINE] Available at: http://www.openhandproject.org/downloads/version1_1/Open%20Hand%20Release%20v1_1.zip *[Accessed 5 Mai 2015]*

2.1.1 3D-printing of the Dextrus robotic hand

The available 3D-printer uses the fused deposition model (FDM) process. This method does not require any solvent and the processing and material handling is easy. After finishing the current layer, the base platform is lowered to be able to deposit the next layer [35]. Hence the maximal printing plane is limited with 25.2 cm in length and 19.9 cm in width, three printing processes are needed, as shown in Figure 5. The chosen layer thickness is 0.2mm and is sufficient for this purpose.

During the printing process assistant structures are needed to be able to print cavities and holes and to have a smooth area where the parts are printed on. Unfortunately, this does not guarantee a faultless outcome as it can be seen in Figure 6. Round cavities of approximately two centimetres in diameter are - despite the printed assistant structures - not easy to accomplish. The construction collapses during the hardening process.

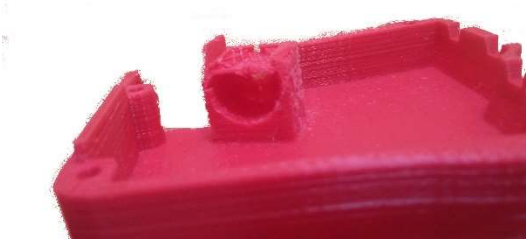

Figure 6: The 3D-printing process is not able to print big round cavities like they are needed for holding the DC-motor

2.1.2 Assembling the Dextrus robotic hand

An instruction, how to build up the Dextrus hand v1.1 is provided at the instructables.com-Website[2]. Each digit performs the flexion and extension by a planetary geared motor. These motors can take a maximum of 12V DC and are able to apply a torque of 8.68 g*cm (0.85 mN*m) to the load. A fully assembled digit is shown in Figure 7.

Figure 7: Example of a fully assembled phalanges II – IV. The motor is positioned at the rear of the finger.

The functionality of the tendons and muscles is substituted by an invisible thread. This monofilament thread is winded on the spool which is attached to the motor shaft. Depending on the rotation direction one of the tensioner is activated and the other one gets loosen and the movement is performed.

The thumb is additionally driven by a servomotor, which requires 5V DC. This servomotor is

[2] *instructables, 2014, Dextrus v1.1 Robotic Hand, [ONLINE] Available at:* http://www.instructables.com/id/Dextrus-v11-Robotic-Hand/ *[Accessed 15 June 2015]*

necessary to perform opposition and reposition and for abduction and adduction in combination with the 12V DC motor. The components for controlling the thumb are hidden in the front part of the Dextrus robotic hand.

The motors for phalanges II-IV are hidden in the back of the Dextrus robotic hand (see Figure 8).

Figure 8: Phalanges II – IV are placed in their housing.

The Arduino Uno is not able to provide the needed power because of is limitations. A driver circuit is needed for the 9V motors. The set is tested with a circuit on a patch panel (see Figure 9).

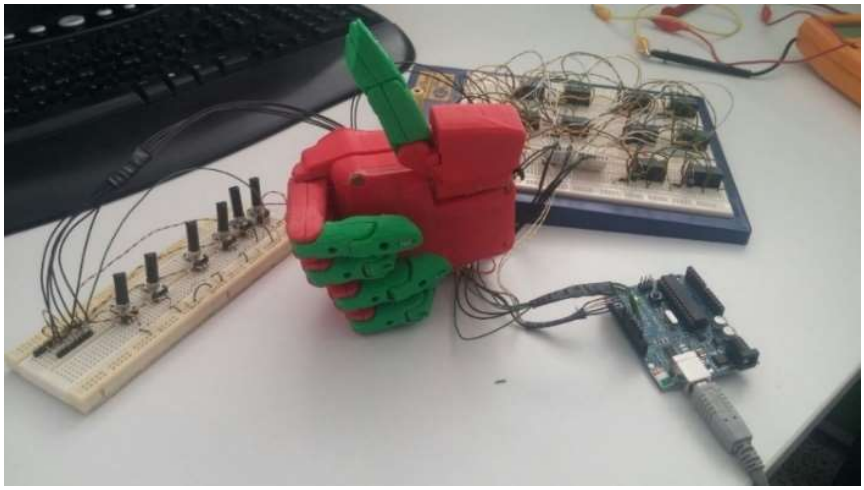

Figure 9: The assembled Dextrus hand with the test board for steering the movements

For usage improvements, designing of a printed circuit board (PCB) follows.

2.2 The Printed Circuit Board

Designing a PCB layout should be done by following PCB design guidelines. There are different design guidelines depending on the kind of circuit which is put onto the board. Hubing Todd (2003)

summarized the main obstacles e.g. circuit noise and disturbances produced by loops which act as antennas. The PCB designed contains only one layer and therefore the noise coupling between power buses must not be taken into account. [36]

The PCB designed for this work contains ten driver circuits which provides the 12V DC motors with the needed power. For every digit and the two different directions being implemented, one example is shown in Figure 10. The inputs of the driver circuit are the output ports of the Arduino, controlled either by the potentiometers or the Matlab/Simulink script. The output of the driver circuit goes back to the Arduino. Depending on which driver circuit was activated, the digit and its movement's direction is determined. The servo motor for opposing or repositioning the thump is controlled directly via the Servo-output Pin of the Arduino.

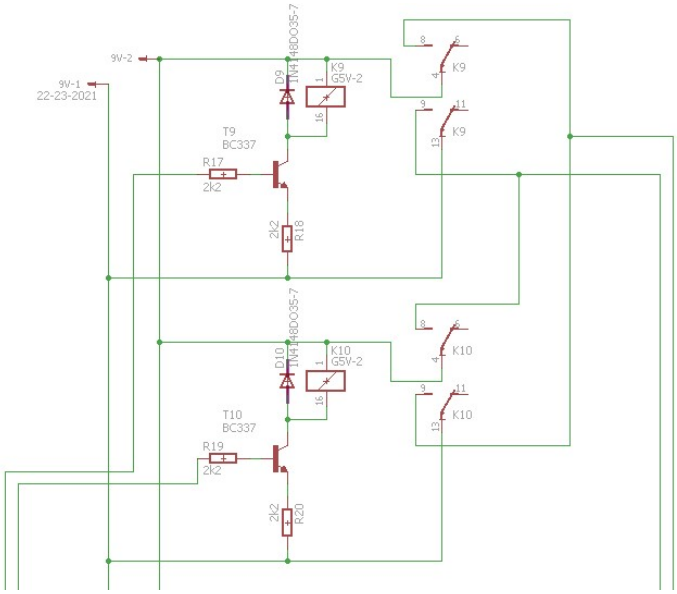

Figure 10: In the figure above the driver circuit for the supination and pronation of the hand is shown. The driver circuit provides the motor with 9V DC voltage. The inputs of the driver circuit (left side in the figure) are output pins of the Arduino board. Depending on the potential one of the relays is activated and the corresponding direction/movement of the hand and its motors is performed.

For testing purposes there is a bank with potentiometers on the PCB (see Figure 11). These are connected to the Analog Input-Ports of the Arduino to control the possible movements of the hand without any other input required. It only needs the written code Appendix B) executed on the Arduino board itself. The changes of the potentiometer's resistant values are translated into changes of the related Dextrus robotic hand's motor and accordingly changes the position of the artificial digits. The input voltage of 5V is provided by the Arduino board.

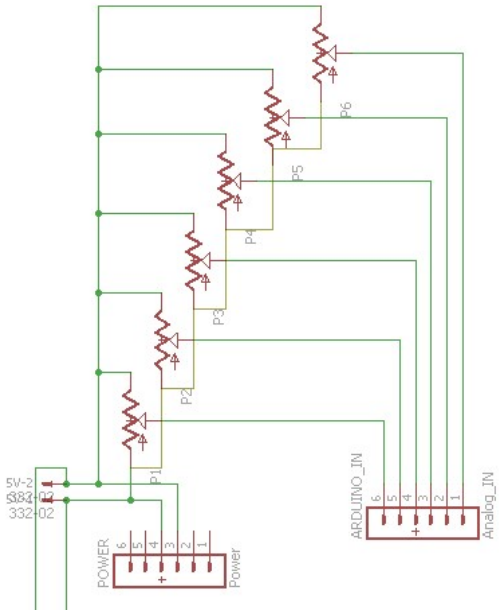

Figure 11: The potentiometers are able to control the Dextrus hand's motors for testing purposes. The testing script has to be uploaded to the Arduino board beforehand. This script translates the changes of the input voltage into interrelated changes of the Dextrus hand's positioning. Hereby the six motors (five for flexing or extending the digits and one for opposing and repositioning the thumb) can be adjusted.

The PCB is shown in Appendix A Printed Circuit Board.

2.3 The BCI-System

Graz-BCI Lab develops the BCI-system used for this thesis. It works with Mathworks Matlab and Simulink (Mathworks Inc., Natick, USA). It is designed to work well with Matlab version 2012b and a 64bit System with Windows 7. The base BCI-System used for this thesis was written by Reinhold Scherer and was adopted by David Steyrl.

The BCI works as follows: The EEG-signal is recorded. A pre-processing step enhances the EEG signal which is affected by artefacts and the volume conduction, a result of the liquor, skull, and scalp. The features are calculated. The three best calculated feature vectors for each of the two classes are taken out of the CSP-matrix for training the linear discriminant analysis (LDA) function. The classifier makes it possible to distinguish between the classes. By filtering the events, it is possible to give feedback to the user through performing a motion by the artificial hand in respect to the given event and the motor imagination.

2.4 The Arduino-module in Simulink and Matlab

Ardunio was invented in Ivrea (Italy) in 2005. It is an open-source prototyping 8-bit platform. The inputs and outputs are commanded by C or C++ code, written with the Arduino Software. It is also possible to use some output pins with the pre-coded PWM. The board used in this thesis is the Arduino Uno. As the BCI-System is working with Matlab and Simulink, the provided support package[3] for controlling the Arduino board by Mathworks is used. In this case the legacy support package had to be installed.

The support packages provide system blocks which interact with the ports of the Arduino. Hence, it is possible to control the ports via matlab scripts, which holds the benefit that the matlab environment can take care of time critical operations without developer interaction. Figure 12 shows the block diagram built in Simulink. The constants “MoveFinger”, “HandEnabled”, “FingersExtended”, “MoveWrist”, and “WristPronated” are controlled by the Matlab script. The Boolean variable “HandEnabled” unlocks the Dextrus hand to be controlled. This is done at the beginning of the feedback session. The variables “FingersExtended” and “WristPronated” are the state variables for the Dextrus robotic hand and are set corresponding to the observed state of the hand at the beginning. The initial position of the artificial hand was all digits extended and the thumb repositioned. A defined starting position is necessary due to the lack of feedback from the Dextrus robotic hand. Depending on the output of the classifier, the binary values for “MoveFinger” and “MoveWrist” are set.

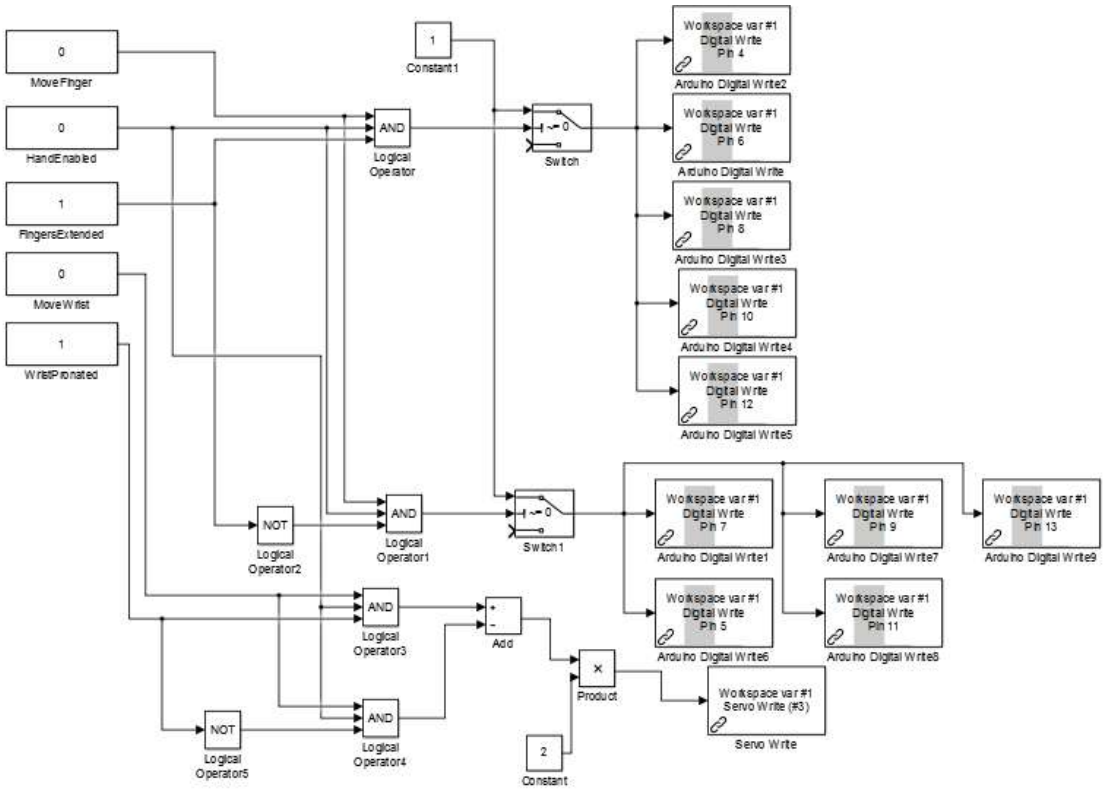

Figure 12: Controlling the Dextrus robotic hand via the Simulink blocks and Matlab script

[3] *MathWorks, 2012, Arduino Support from Simulink, [ONLINE] Available at:* http://uk.mathworks.com/hardware-support/arduino-simulink.html?s_tid=gn_loc_drop, *[Accessed 2 September 2015*

2.5 BCI Experiment

The BCI-system built in this thesis is cue-based. There are two classes which control the Dextrus robotic hand. One class represents the supination or pronation of the right hand and the other class represents the flexion or extension of the right hand's fingers. As the built hand is not able to perform a supination and a pronation by itself, this movement is demonstrated to the subject by opposing and repositioning of the thumb. Additional to the feedback of the artificial hand, a bar presents the output of the classifier on the screen. Depending on the task and the distance calculated by the classifier, this bar either grows along the positive y-axis (event for moving the fingers) or increases along the positive x-axis (event for turning the hand). If the classifier is above the given threshold in the defined time interval, the previously white coloured bar turns green and the hand performs the movement.

2.5.1 Subjects and instructions to subjects

Three female and five male participants attended the experiment. The age of the participants was between 24 and 32 years (average 27.5 years). One male subject was left-handed and had participated in a different BCI-study in the past, the others were right-handed and naïve to BCI-studies. Every participant had normal or corrected-to-normal vision. The subjects were seated in an armchair about 100cm in front of a computer screen at eye level. Before the start of the experiment, the participants were precisely instructed. A written instruction was presented to the subjects. The main idea of a BCI-system was explained, the movement imaginations to be used were shown and explained in detail. Thereby, the participants were told to rest their arm on the adjustable armrest during the experiment. The fingers were extended and the forearm in pronated position. The angle between the upper and the lower arm was about 90 degrees. This was necessary to exclude rotations performed in the shoulder and the predefined setting ensured more comparable data. The exact timing of the paradigm was clarified. Prior to the first motor imagery session, the subjects had to execute the different movements (opening and closing the hand or rotating the lower arm) according to the cues presented. These cues could be either an arrow pointing to the left and right or pointing to the top and bottom. The first possible cue (horizontal arrow) indicated the opening and closing of the hand and the latter (vertical arrow) illustrated the rotation of the lower arm. In the following runs the subjects were instructed to imagine the previous executed movements in consonance with the presented cue. These runs were training sessions without feedback. Between the runs the participant could have a short break. After absolving the training session, a run with feedback was performed.

Every movement was instructed to be done periodically and repeatedly.

Two male and one female subject took part in the extended study. It comprises a task of distinguishing left vs. right hand movement by first motor execution and second motor imagery. These three

participants got additional instructions and this sub experiment was done before the main experiment. This experiment was performed to prove the integrity of the BCI-system.

The offline BCI with the motor imagery task prepared the subjects and the BCI-system for the following experiment which was the main target for this thesis. This task was done with online classification and feedback. The feedback was given by the Dextrus robotic hand and a bar to indicate the distance of the classifier. The bar changed the colour from the standard colour white to green, if the given threshold and other requirements were matched. These requirements were of statistical manner so that not every short burst over the threshold would perform an action. It had to be 60% of the time above the threshold. As already mentioned, a supination or pronation of the artificial hand was not possible. In this case, the thumb would perform an opposition or reposition movement. The fingers II to IV represented the correct classification of the finger's motor imagery and a contemporaneous activation of the robotic hand's fingers took place (see Figure 12).

The participants were instructed to be focused on the task, voiding eye movement and swallowing, albeit not fully preventable but as far as possible.

2.5.2 Paradigm

The starting point of the experiment was cued by a fixation cross centred on the screen. The attention was focused by a beep after two seconds. In second three after the start, the cue stimulus was shown. In this thesis the cue stimulus was an arrow pointing either up and down or left and right. This arrow was shown for 1.25 seconds. The presented visual cues were presented in a random order. After a total of eight seconds the trial ended and a new one started after a varying break (to prevent adaption) of two to three seconds. The scheme of the paradigm is shown in Figure 13.

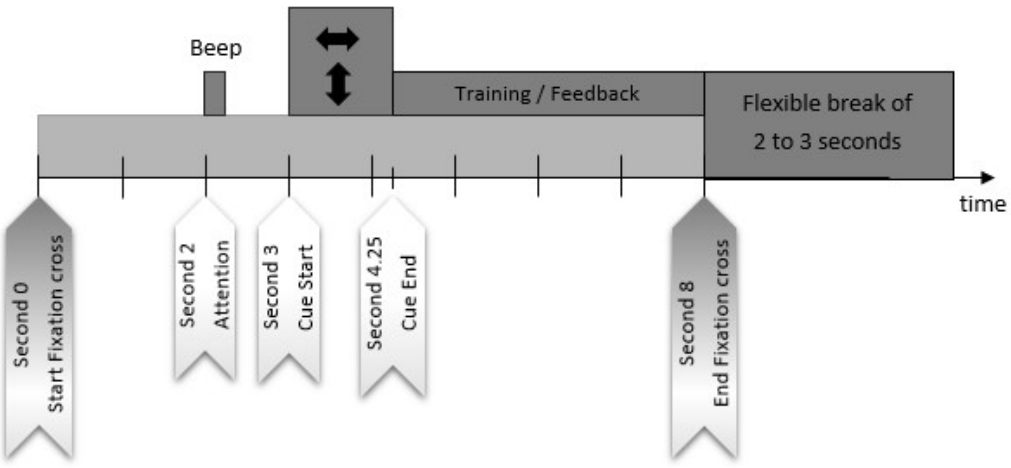

Figure 13: Scheme of the Paradigm

One run of an experiment consisted of 40 trials giving 20 trials for each class and are presented randomly. In case of the imagery of hand and finger movements there were 3 runs which means a total sum of 120 trials and therefore 60 trials for each class.

2.5.3 Signal recording

The EEG was recorded via 61 electrodes. Three additional electrodes measured the EOG. The positioning of the 61 EEG-channels is shown in Figure 14. The localisation of the EEG electrodes was determined using ELPOS from zebris [zebris Medical GmbH, Isny, Germany]. The points fidnz, fidt10 and fidt9 are the reference coordinates for ELOPS.

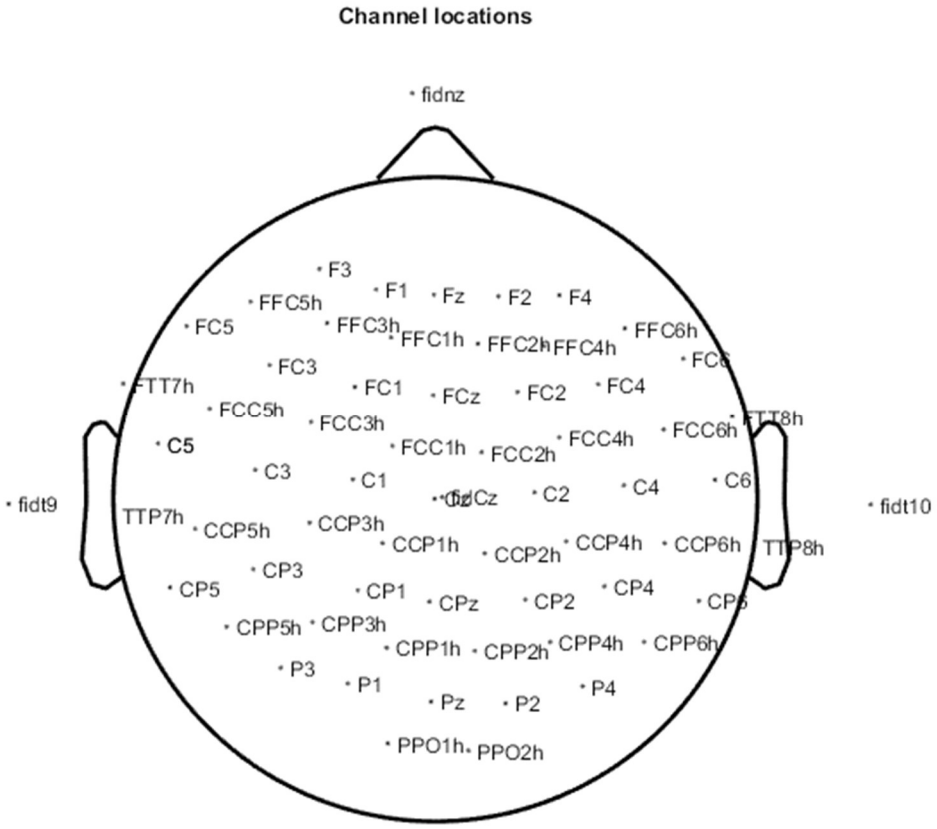

Figure 14: Position of the electrodes

The sampling frequency was 512 Hz. A Chebyshev filter was applied to each channel with a frequency band of 0.01Hz to 200Hz. The notch filter of 50Hz was on. The ground electrode was at AFFz and the left ear lobe was the reference.

2.5.4 Offline BCI

During the offline BCI session, subjects were first told to actively execute one of the two different movements, which were shown on the screen. The next run was the part where subjects imagined movements and the main part of the session.

2.5.5 Online BCI

For the online BCI, the data which was recorded during the offline BCI was processed via the CSP filter and LDA classifier. The timeframe for the CSP was set during the training/feedback period, which is shown in Figure 13. After processing, the paradigm was started in a similar way as in the offline BCI. The difference of the online BCI compared to the offline BCI was such that during the training period feedback was shown to the subject. In this thesis that was done in two ways. First, the bionic hand showed the feedback. The movement of the fingers were able to be performed by the Dextrus robotic hand, the movement of the wrist was shown by the opposition and reposition of the thumb. In addition to the artificial hand, there was a bar on the screen, which was extended in the direction determined by the classifier output. The length of this bar showed the distance the classifier calculated between the two classes. In this thesis, the bar could grow from the centre to the bottom and from the centre to the right. The extension and flexion of the fingers corresponded to a bottom-growing bar and the supination and pronation corresponded to a bar which grew to the right. A correct classification was shown by a green bar which indicated the movement of the hand.

2.5.6 Analysis

The analysis of the EEG-data was done with Matlab scripts. For artefact rejection a statistical approach (standard deviation, variance, kurtosis) [37] was computed first but at the end a visual inspection of the data was done and the trials were rejected manually.

2.5.6.1 ERD/ERS

The ERDS-Maps were calculated by adapting the provided scripts included in the Graz-BCI-system. To obtain the time-frequency maps, the data was segmented with respect to the visual cue onset. The three second lasting timeframe before this onset and five seconds later held the information of the entire trial. The EEG data of each channel was filtered in the selected frequency band. Small-Laplace filtering was applied to the data. The eight second lasting segments were analysed in a frequency band between 4 and 50 Hz with respect to the reference interval lasting 1.5 to 2.5 seconds prior of the onset of the visual cue [17]. This time window excludes the possible arousal caused by the auditory signal (Beep).

2.5.6.2 K-fold cross-validation

The test data estimates the classification error. Therefore, the data is split into two subsets. One is the testing and the other the training-data set for the cross-validation. During k-fold cross-validation, the classifier is tested and trained k times. The resulting k error rates are averaged and the overall error is given by

$$\boldsymbol{err} = \frac{\mathbf{1}}{\boldsymbol{k}} \sum_{\boldsymbol{i=1}}^{\boldsymbol{k}} \boldsymbol{err_k} \qquad (9)$$

2.5.6.3 Cohen's Kappa coefficient

This statistical measure takes the agreement occurring by chance into account. The equation is as follows:

$$\kappa = \frac{p_0 - p_e}{1 - p_e} \quad (10)$$

The variable p_0 describes the relative observed agreement of the classifier for the two classes and p_e is the hypothetical probability of chance agreement. The value varies between -1 and +1, whereas 1 implies a perfect agreement/classification and -1 is the worse than random state. Random is given if kappa is 0. [38] The values for calculating kappa are derived like shown in Table 2.

Table 2: Confusion matrix for observed data

Confusion matrix **observed**		PREDICTED	
		Finger movement	Wrist movement
ACTUAL	Finger movement	a_o	b_o
	Wrist movement	c_o	d_o

The values a_o, b_o, c_o, d_o. which are shown in Table 2, are the results, while comparing actual and predicted events. N_o is the sum of all events. The observed agreement is derived by

$$p_0 = \frac{a_0 + d_0}{N_0} \quad (11)$$

Table 3: Confusion matrix for expected data: The formulas for computing the expected cell frequencies are shown here.

Confusion matrix **expected**		PREDICTED	
		Finger movement	Wrist movement
ACTUAL	Finger movement	$(a_o+b_o)(a_o+c_o)/N_o$	$(a_o+b_o)(b_o+d_o)/N_o$
	Wrist movement	$(c_o+d_o)(a_o+c_o)/N_o$	$(c_o+d_o)(b_o+d_o)/N_o$

The Confusion matrix of the expected agreement and the calculation of the corresponding expected cell frequencies is shown in Table 3. Finally, the hypothetical probability of chance agreement can be calculated:

$$p_e = \frac{Expected(a) + Expecte\ (d)}{N_0} \quad (12)$$

The Cohen's Kappa coefficient are characterized by values as follows [39]:

κ= <0: no agreement

κ= 0 to 0.20: slight agreement

κ= 0.21 to 0.40: fair agreement

κ= 0.41 to 0.60: moderate agreement

κ= 0.61 to 0.80: substantial agreement

κ= 0.81 to 1: almost perfect agreement

3 Results

In this chapter the results of the BCI-system built for this thesis are presented.

In sub chapter 3.1 and 3.2 the time-frequency maps (ERDS) for left versus right hand movement are shown. The first three participants did an experiment lasting 40 trials per class experiment of right versus left hand motor execution (see chapter 3.1) and a 40 trials per class lasting experiment of right versus left hand motor imagery (see chapter 3.2).

Sub chapter 3.3 shows the main results, which were the goal of this thesis, to control the artificial hand with intentional controls. These results are based on runs with summed up 120 trials per class. The result of the bootstrapping significance test is shown after the presentation of the ERDS maps.

For each of the above described results, one representative figure is shown in the results chapter. All different results can be found on the CD provided with this thesis.

After presenting the ERDS maps, more statistics are shown. The k-fold cross-validation and the Cohen's kappa coefficients are given in the tables for every subject.

3.1 Time – frequency maps of right and left hand motor execution

Figure 15 shows the ERD/S patterns of repetitive right hand motor execution performed by subject 2.

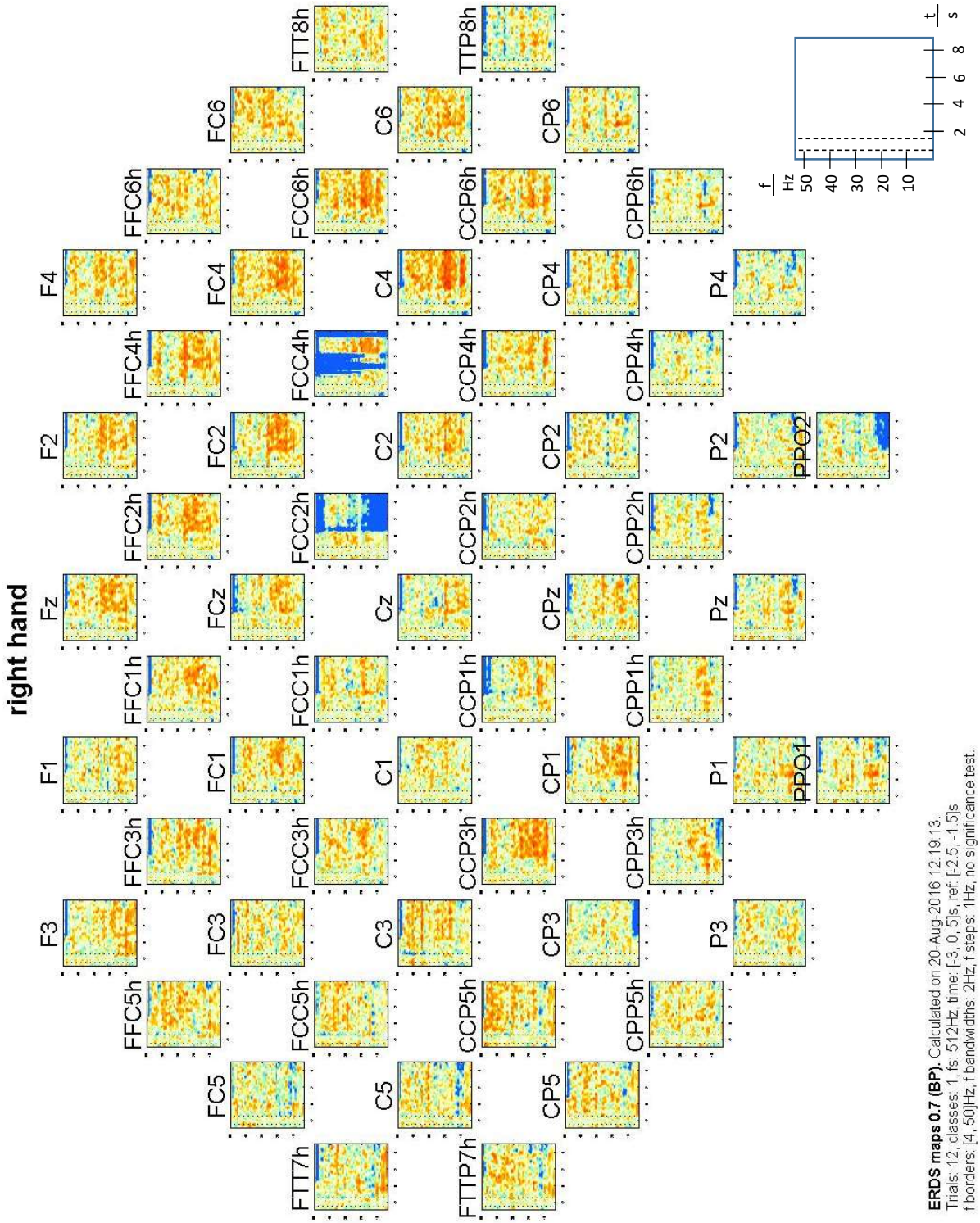

Figure 15: The figure above shows the ERDS of repetitive right hand motor execution. The movements were performed by Subject 2. It is representative for all of the three participants who performed this small test. The data was filtered between 4 and 50Hz and CAR filter was applied. The rejection of trials with artefacts leads to a smaller number of trials and therefore also to smaller significance. Another pitfall was the unintentional cue which was used. The right/left arrowed cue had to be "translated" into movement of the right hand. More than that, the awareness of where left and right is, was in addition to the previous problem, another reason for mistakes and therefore resulting in data like shown above.

Figure 16 shows the ERD/S patterns of repetitive left hand motor execution performed by subject 2.

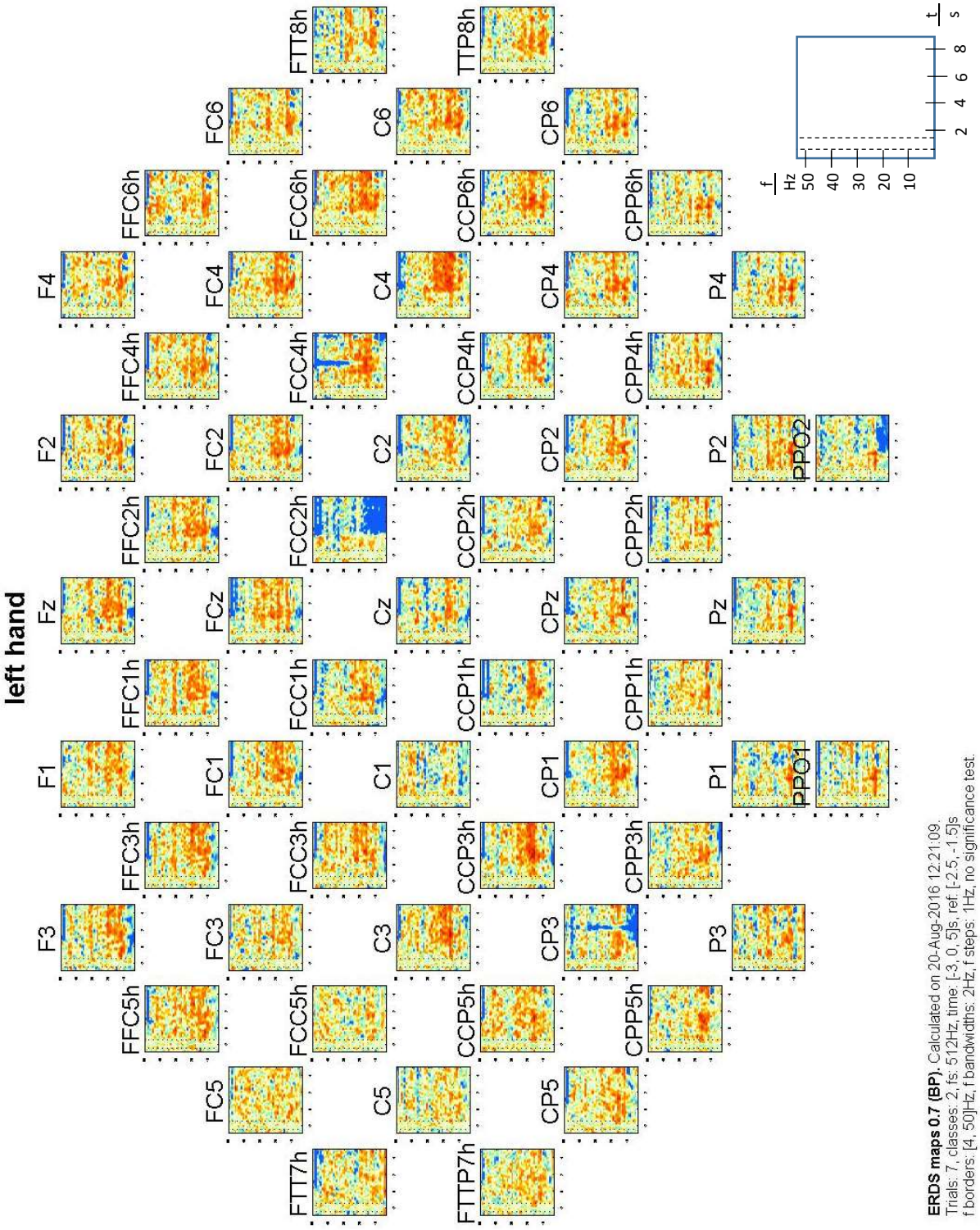

Figure 16: The figure above shows the ERDS of repetitive left hand motor execution. The movements were performed by Subject 2. It is representative for all of the three participants who performed this small test. The data was filtered between 4 and 50Hz and CAR filter was applied. The maps show bands around 10Hz and 20Hz. The rejection of trials with artefacts leads to a smaller number of trials and therefore also to smaller significance. Another pitfall was the unintentional cue which was used. The up/down arrowed cue had to be "translated" into movement of the left hand. More than that, the awareness of where left and right is, was in addition to the previous problem, another reason for mistakes and therefore resulting in data like shown above.

3.2 Time – frequency maps of right and left hand motor imagery

Figure 17 shows the ERD/S patterns of repetitive right hand motor imagery performed by subject 2.

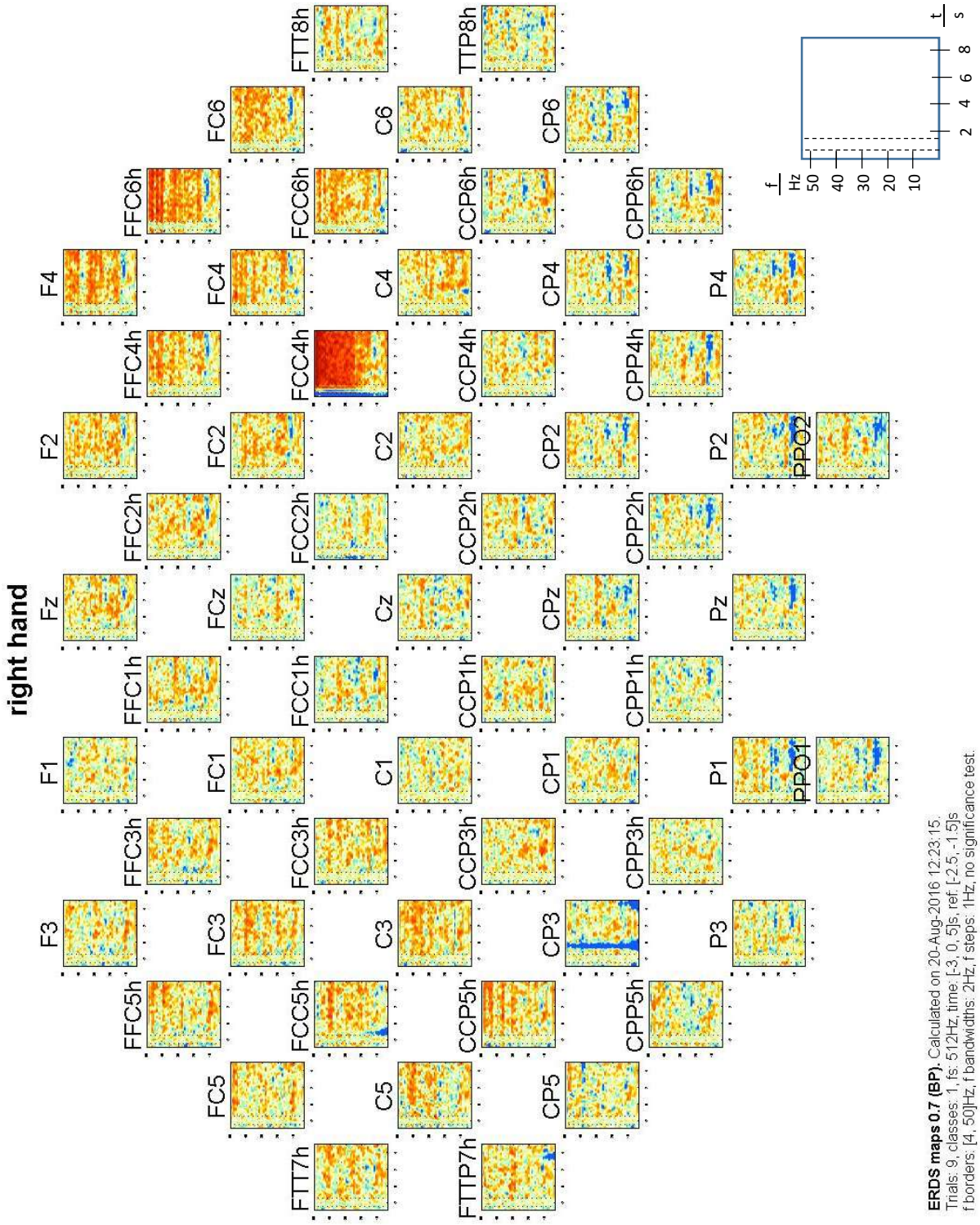

Figure 17: The figure above shows the ERDS of repetitive right hand motor imagery. The motor imagery was performed by Subject 2. It is representative for all of the three participants who performed this small test. The data was filtered between 4 and 50Hz and CAR filter was applied. The rejection of trials with artefacts leads to a smaller number of trials and therefore also to smaller significance. Another pitfall was the unintentional cue which was used. The up/down and right/left arrowed cue had to be "translated" into left and right. More than that, the awareness of where left and right is, was in addition to the previous problem, another reason for mistakes and therefore resulting in data like shown above.

Figure 19 shows the ERD/S patterns of repetitive left hand motor imagery performed by subject 2.

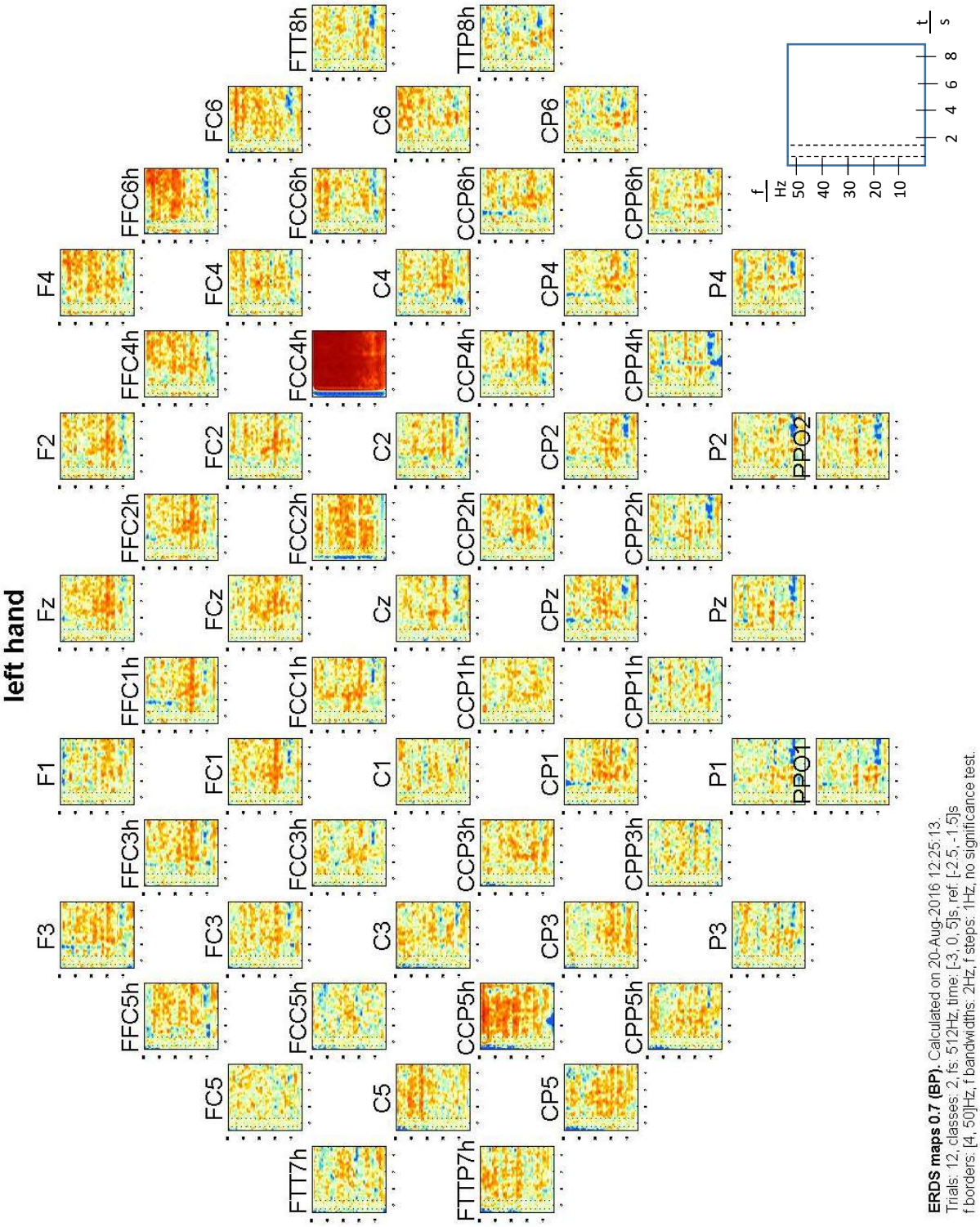

Figure 18: The figure above shows the ERDS of repetitive left hand motor imagery. The motor imagery was performed by Subject 2. It is representative for all of the three participants who performed this small test. The data was filtered between 4 and 50Hz and small CAR filter was applied. The maps show bands around 10Hz and 20Hz. These bands are not as present as the ERDS maps show during motor execution. The rejection of trials with artefacts leads to a smaller number of trials and therefore also to smaller significance. Another pitfall was the unintentional cue which was used. The up/down and right/left arrowed cue had to be "translated" into left and right. More than that, the awareness of where left and right is, was in addition to the previous problem, another reason for mistakes and therefore resulting in data like shown above.

3.3 Time – frequency maps of forearm and fingers motor execution

Figure 19 shows the ERD/S patterns of repetitive supinating and pronating the right hand performed

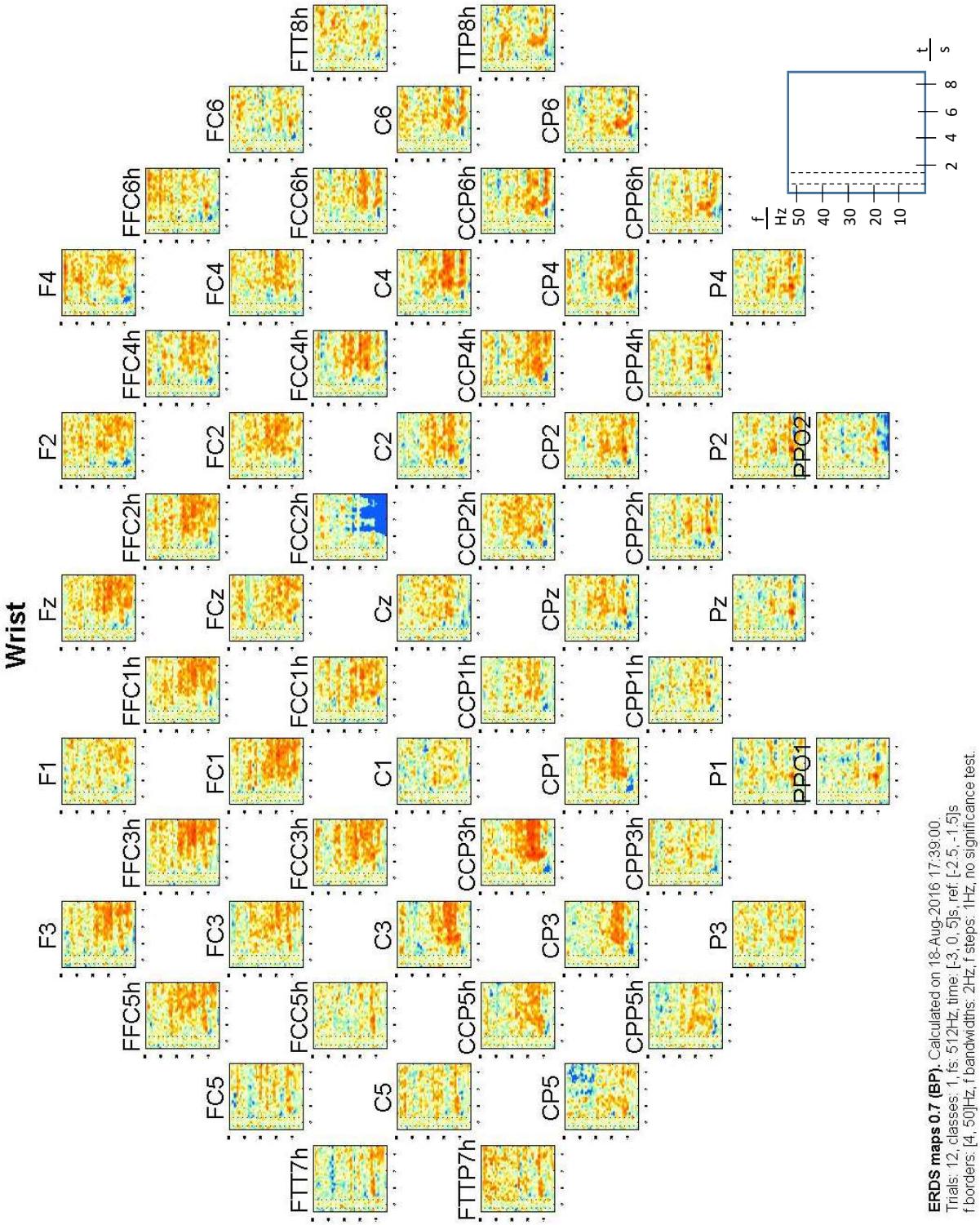

Figure 19: The figure above shows the ERDS maps of motor execution of repetitive pronation/supination of the right hand performed by Subject 2. The data was filtered between 4 and 50Hz and CAR filter was applied. Bands around 10 and 20 Hz are visible.

Figure 20 shows the ERD/S patterns of repetitive flexing and extending the right hand's fingers performed by subject 2.

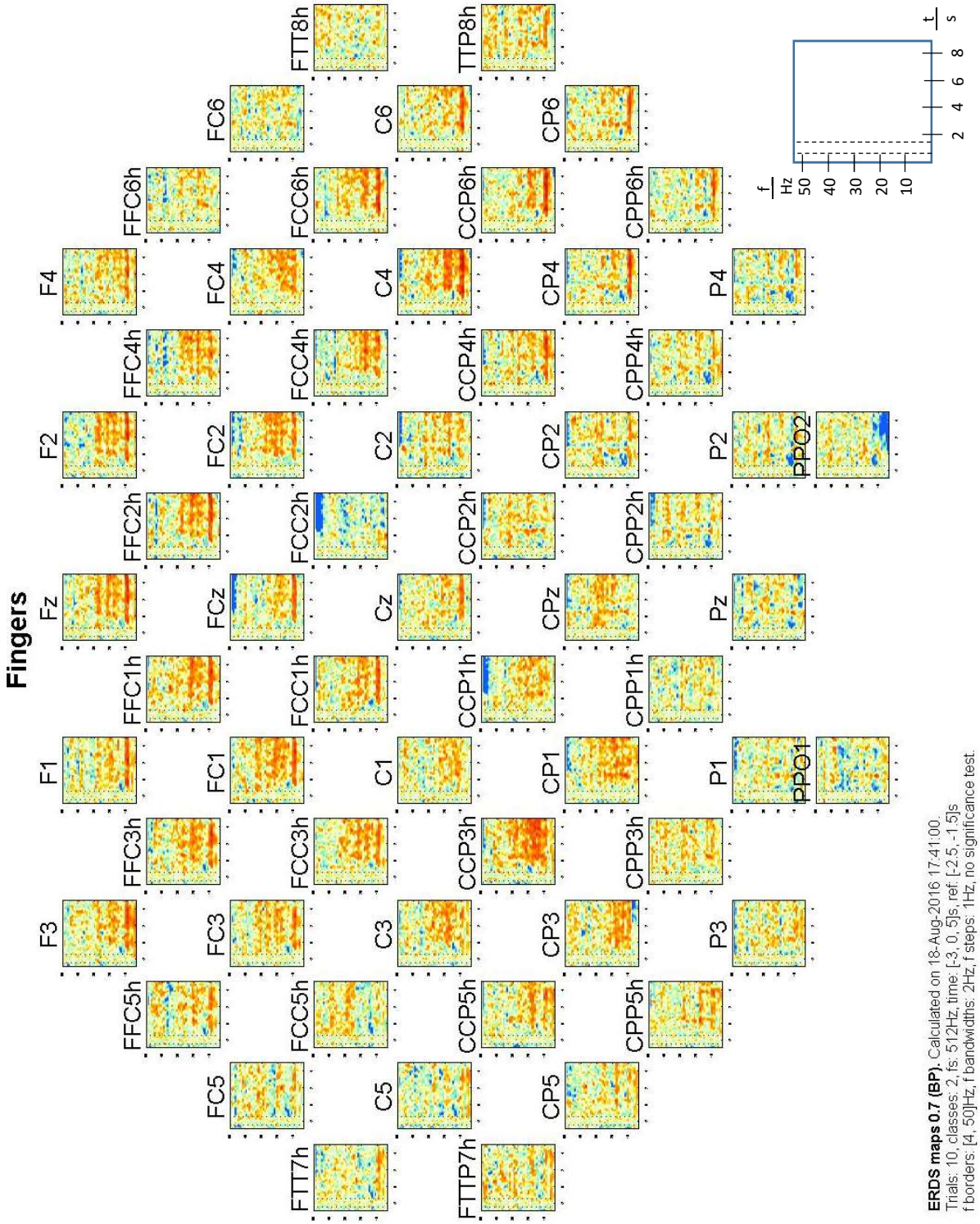

Figure 20: The figure above shows the ERDS maps of motor execution of repetitive flexion/extension of all fingers of the right hand performed by Subject 2. The data was filtered between 4 and 50Hz and CAR filter was applied. Bands around 10 and 20 Hz are visible.

3.4 Time – frequency maps of forearm and fingers motor imagery

Figure 21 shows the ERD/S patterns of imagined repetitive supination and pronation of the right hand performed by subject 2.

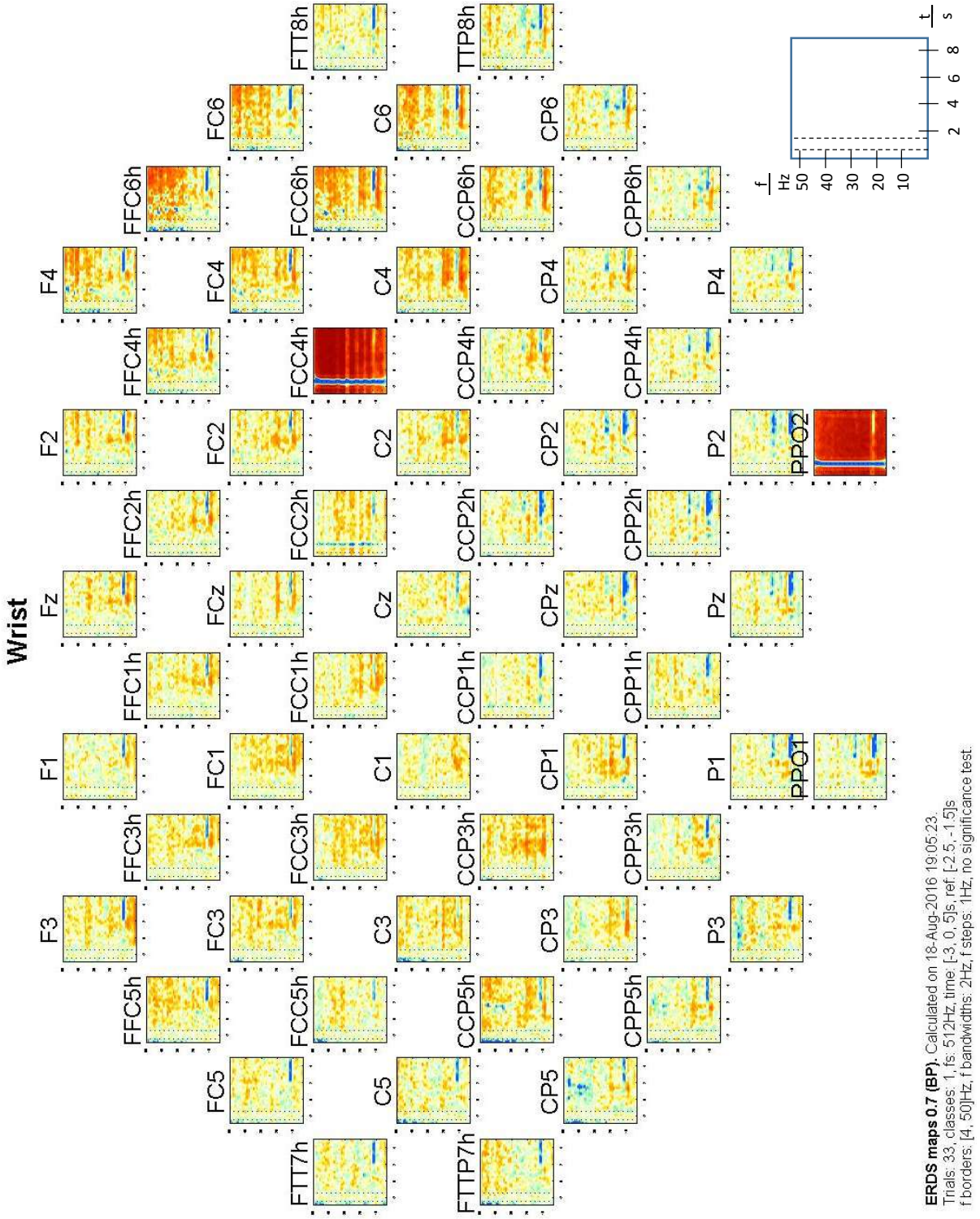

Figure 21: The ERDS maps of motor imagery of repetitive pronation/supination of the right hand are shown. The motor imagery was performed by subject 2. The data was filtered between 4 and 50Hz and CAR filter was applied.

Figure 22 shows the ERD/S patterns of imagined repetitive flexion and extension of the right hand's fingers performed by subject 2.

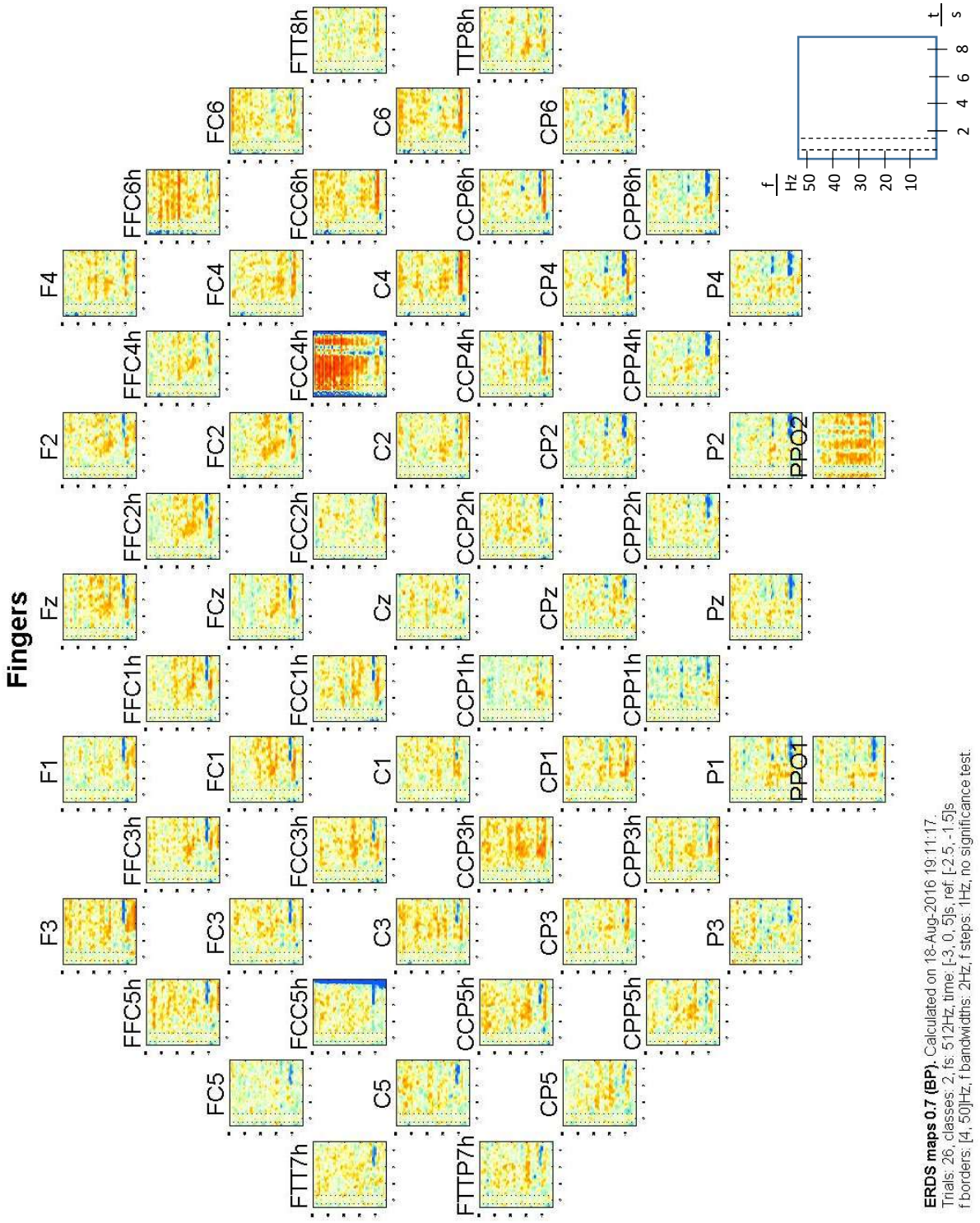

Figure 22: The ERDS maps of motor imagery of repetitive flexion/extension of the right hand's fingers are shown. The motor imagery was performed by subject 2. The data was filtered between 4 and 50Hz and CAR filter was applied.

3.5 Time – frequency maps: Significance test of repetitive forearm and finger movement imagery with Bootstrap

Figure 23 shows the significant ERD/S patterns (Bootstrap significance test (α=0.05)) of repetitively imagined supination and pronation of the right hand performed by subject 2.

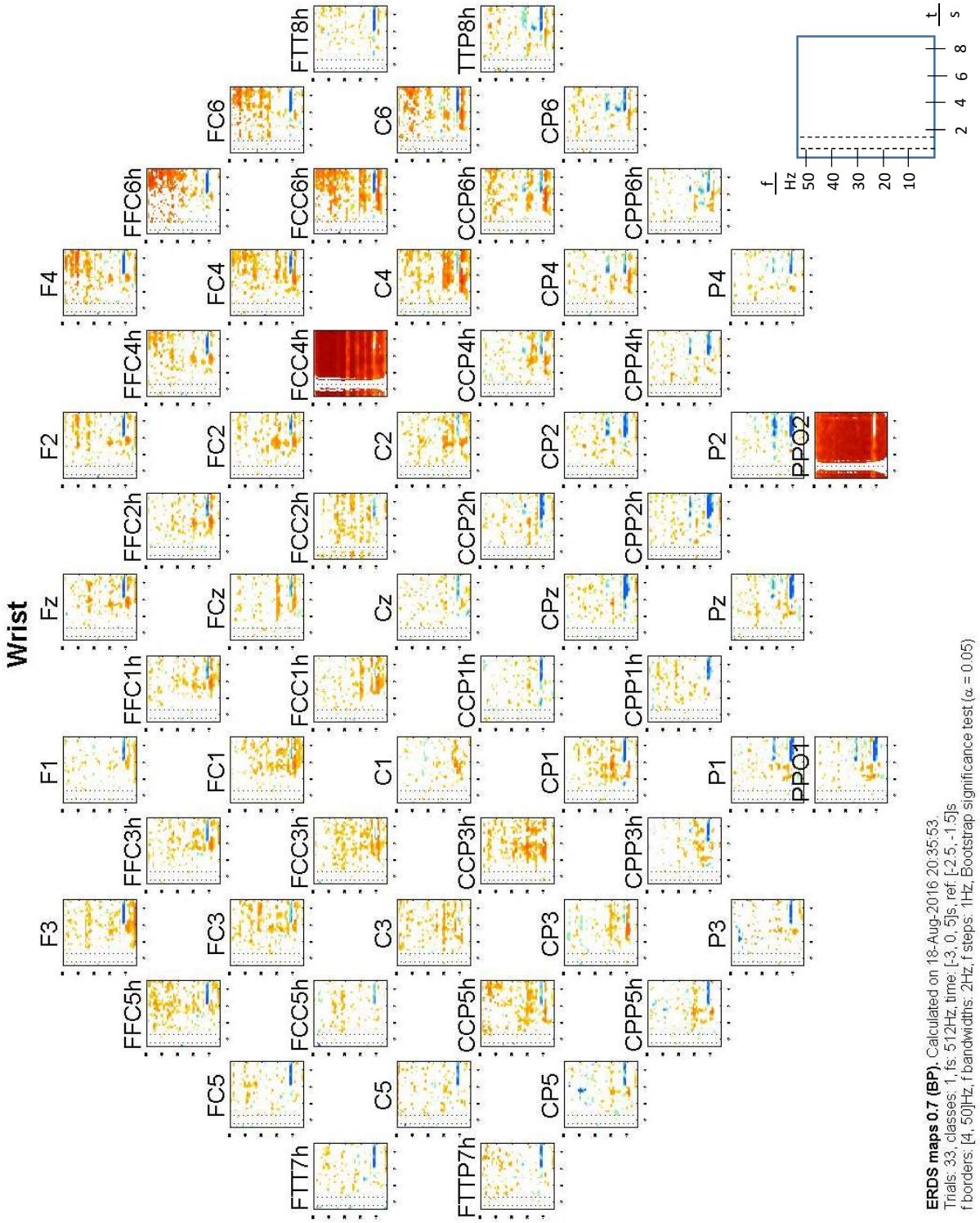

Figure 23: The figure above shows the ERDS patterns of right wrist movement imagery with the Bootstrap significance test (α=0.05).

Figure 24 shows the significant ERD/S patterns (Bootstrap significance test (α=0.05)) of repetitively imagined flexion and extension of the right hand's fingers performed by subject 2

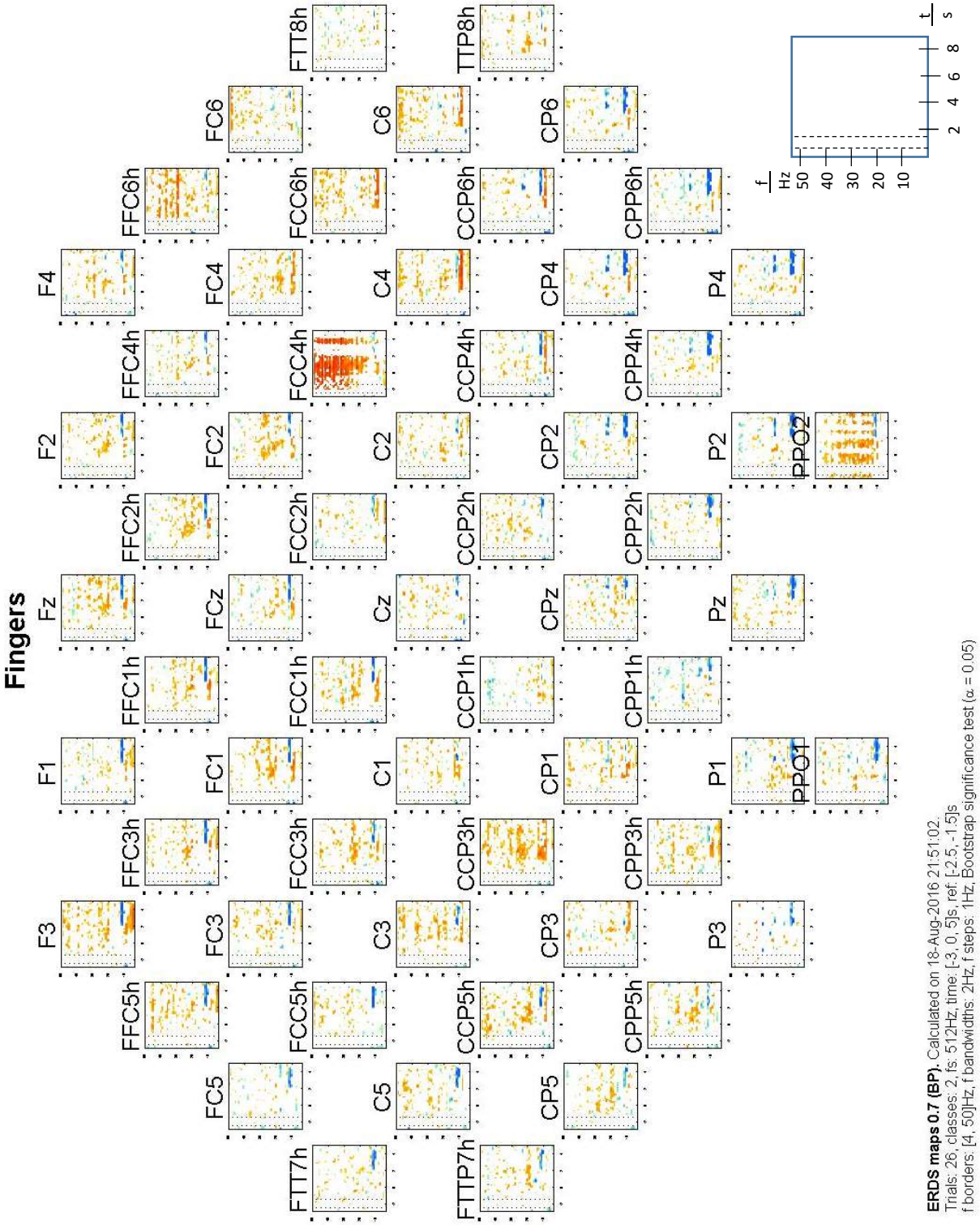

Figure 24: The figure above shows the ERDS patterns of right hand's fingers movement imagery with the Bootstrap significance test (α=0.05).

3.6 Time – frequency maps of forearm and fingers motor imagery with feedback

Figure 25 shows the ERD/S patterns of imagined repetitive supination and pronation of the right hand with feedback performed by subject 6.

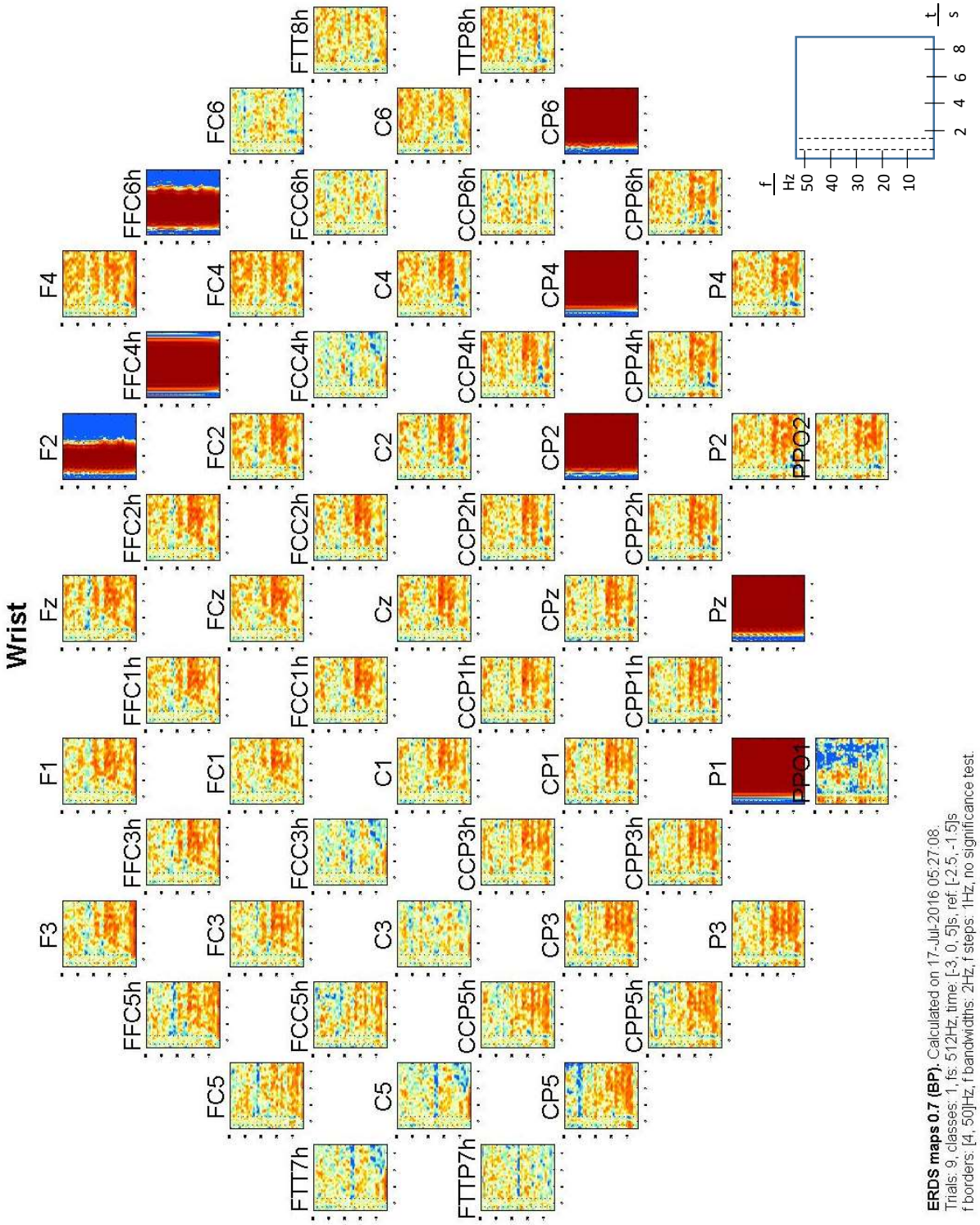

Figure 25: The figure above shows the ERDS patterns of right hand's movement imagery with feedback performed by Subject 6. The data was filtered between 4 and 50Hz and CAR filter was applied. Bands around 10 and 20 Hz are visible.

Figure 26 shows the ERD/S patterns of repetitively imagined flexion and extension of the right hand's fingers with feedback performed by subject 6.

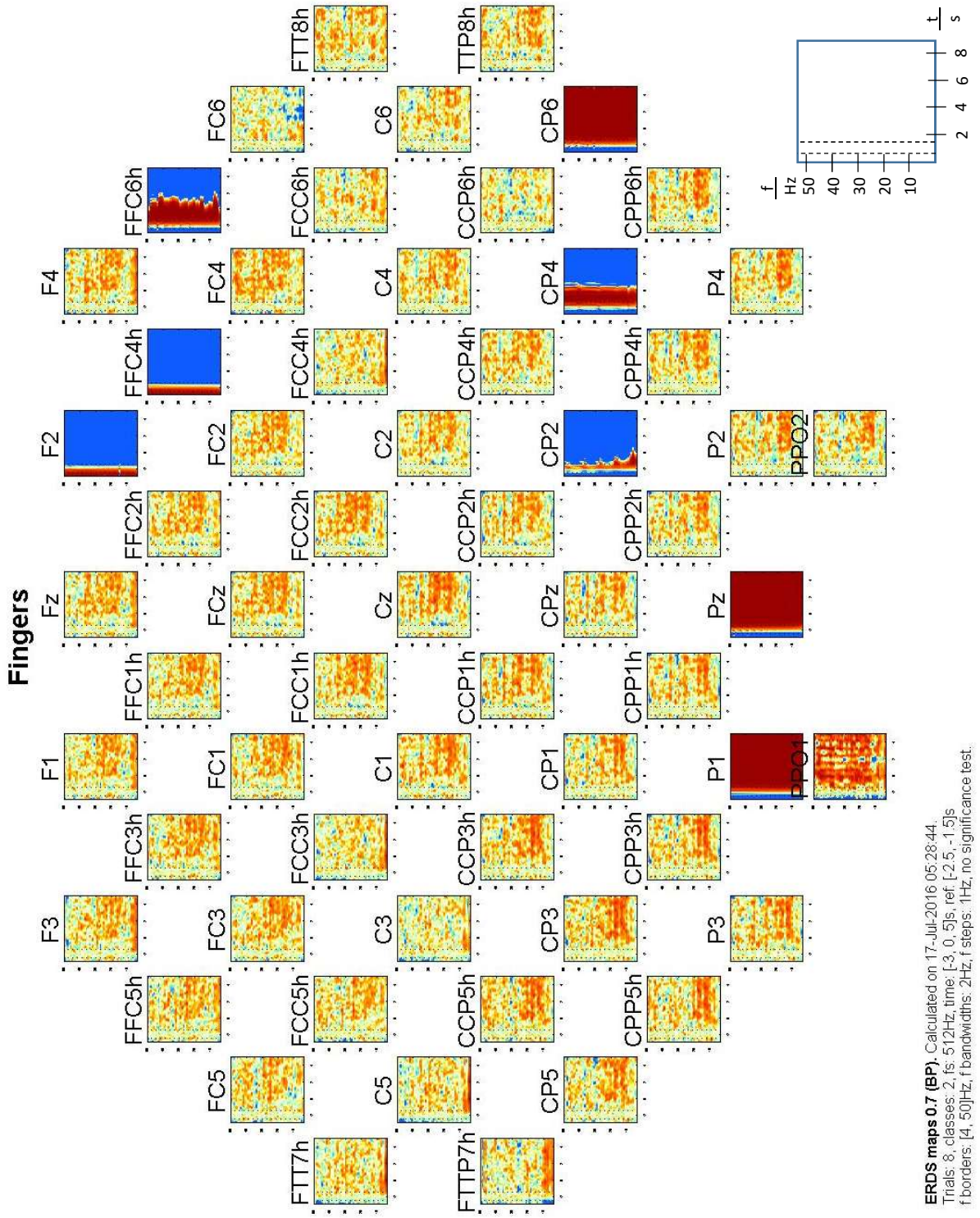

Figure 26: The figure above shows the ERDS patterns of right hand's fingers movement imagery with feedback performed by Subject 6. The data was filtered between 4 and 50Hz and CAR filter was applied. Bands around 10 and 20 Hz are visible

3.7 Cross-validation and Cohen's kappa coefficient

The following Cohen's kappa coefficients were obtained using cross-validation of the data recorded during motor imagery of the pronation/supination of the right hand and flexion/extension of the right hand's fingers. The following table shows the average kappa derived with 5-fold and 10-fold cross-validation for all seven participants' EEG. Table 4 shows κ (kappa) for every channel filtered between 8 to 30 Hz. The difference of 5 to 10-fold cross-validation becomes here clearly visible. Table 5 shows the kappa coefficient of data after performing a small Laplacian reference.

Table 6 shows the results for kappa of data filtered between 8 and 30 Hz and CAR applied.

Table 4: Kappa coefficients: The Cohen's kappa coefficients calculated during k-fold-cross validation of data filtered between 8 to 30Hz are compared. The average κ is the average over every single fold.
The data used is the offline data and online data with feedback of every participant (S1 to S8) during motor imagery of the right hand's wrist and fingers. The average κ is the average of all found kappas during the cross validation of the dataset of the corresponding user. Each channel's data was taken as measured without any common reference filtering.

5-fold cross validation of EEG data (Monopolar; filtered: 8-30Hz)								
	S1	**S2**	**S3**	**S4**	**S5**	**S6**	**S7**	**S8**
Average κ	-0.21	-0.54	-0.10	-0.46	-0.61	-0.46	-0.49	-0.68*
Standard-deviation	0.34	0.23	0.40	0.30	0.30	0.15	0.42	0.288*
10-fold cross validation of EEG data (Monopolar; filtered: 8-30Hz)								
	S1	**S2**	**S3**	**S4**	**S5**	**S6**	**S7**	**S8**
Average κ	-0.54	-0.27	-0.69	-0.67	-0.68	-0.38	-0.60	-0.65*
Standard-deviation	0.41	0.30	0.40	0.39	0.52	0.36	0.26	0.50*
								*offline data only

Table 5: Kappa coefficients: The Cohen's kappa coefficients calculated during k-fold-cross validation of data filtered between 8 to 30 Hz are compared. The average κ is the average over every single fold.
The data used is the offline data and online data with feedback of every participant (S1 to S8) during motor imagery of the right hand's wrist and fingers. The average κ is the average of all found kappas during the cross validation of the dataset of the corresponding user. Small Laplacian reference was computed.

10-fold cross validation of EEG data (small Laplacian; filtered: 8-30Hz)								
	S1	**S2**	**S3**	**S4**	**S5**	**S6**	**S7**	**S8**
Average κ	-0.46	-0.30	-0.58	-0.93	-0.65	-0.25	-0.59	-0.76*
Standard-deviation	0.46	0.30	0.54	0.41	0.39	0.14	0.38	0.40*
*offline data only								

Table 6: Kappa coefficients: The Cohen's kappa coefficients calculated during k-fold-cross validation of data filtered by a bandpass at 8Hz to 30Hz. The average κ is the average over every single fold.
The data used is the offline data and online data with feedback of every participant (S1 to S8) during motor imagery of the right hand's wrist and fingers. The average κ is the average of all found kappas during the cross validation of the dataset of the corresponding user. CAR was computed for every channel.

10-fold cross validation of EEG data (CAR; filtered: 8-30Hz)								
	S1	**S2**	**S3**	**S4**	**S5**	**S6**	**S7**	**S8**
Average κ	-0.52	-0.12	-0.64	-0.13	-0.58	-0.82	-0.22	-0.54*
Standard-deviation	0.45	0.21	0.45	0.08	0.46	0.29	0.31	0.38*
*offline data only								

4 Discussion

In this part of the thesis, the findings that were presented in Chapter 3 will be discussed.

4.1 Experiment

The right and left hand movement-experiment was done to give a quick introduction to the BCI-System to three participants. Therefore, the number of trials was limited because the length of an experiment is crucial, like the findings imply (discussed in detail later). This run was done once and with 20 trials per class. The cue indicating the side to be imagined or performed was not intentionally. It was the same which was used for the further investigations (up/down and left/right). This resulted in confusions like the participants had on the one hand the problem to distinguish the side which was meant and on the other hand it was easy to do the wrong execution or imagination and be aware of it during or after the trial. The strict time schedule was a critical factor too and so this extra experiment got dismissed for the other participants and the focus was on the main goal for this thesis.

The number of trials for the motor imagery of the wrist and finger movements was chosen to be 120. This means that there were 60 trials per class. This corresponds to the findings which dealt with the statistics of EEG-signals. [40] This number was reduced by rejecting trials which were affected by artefacts like swallowing or other muscle activities. After computing the data of the first five participants and finding out that the number of trials which were not affected by muscle activity or had too much noise of other sources, an additional run was recorded. This means that for subject 6, 7, and 8 80 trials per class were available. Nevertheless, this could not improve the results because the length of the experiment was stretched about the amount of time for additional 40 trials. The trials later on in the session of each participant got more affected by all kinds of artefacts. Visual compared to automatic rejection by statistical calculations had almost the same results. There was no artefact rejection during online BCI. The experiment ended with a single run with feedback consisting of 20 trials per class.

4.1.1 ERDS maps

Whereas there are bands visible during motor execution (Figure 15 and Figure 16) of the right and left hand between 8 to 12 Hz, 15 to 20Hz and 20 to 25Hz and as well during motor imagery (Figure 17 and

Figure 18). These frequency bands are also visible in the ERDS maps for the hand-movements, which are the main goal for this thesis. The supination or pronation of the right hand and flexion or extension of the fingers of the right hand is shown in Figure 19 and Figure 20. While there are more clear bands in the same frequency range than previously discussed for hand movements, the bands are not that lucid during kinaesthetically imagine making that movement as shown in Figure 21 and Figure 22. The difference in activation corresponds to findings even in ECoG studies and is caused by the larger portion of neurons needed during active movement. Just a subset of neurons which do not induce actual movement are recruited during motor imagery [41].

Figure 23 and Figure 24 show the significance test with bootstrapping. This approach is a method of resampling. It is obvious that hardly any significant sample could be found during bootstrapping, but there are bands in the range discussed above. The significance difference ($p<0.05$) is shown in these figures. There are some differences visible. The significance difference $p<0.01$ shows varieties in the frequency bands too but is not shown in the figures.

The ERDS maps of the run with feedback is shown in Figure 25 and Figure 26. It is noticeable that there are bands in the already described frequency bands visible. Some electrodes failed during the experiment and as a result no clear information is visible for these electrodes. An additional source of artefacts is the feedback itself. The arousal is caused by the moving of the hand or the bar on the screen. The excitement caused by these representations of being able to control things with the own mind was already obvious during the experiments. This distraction leads to more eye movements and higher EMG activity.

4.1.2 Cross-validation and Cohen's kappa coefficient

The results of k-fold cross-validation and Cohen's kappa coefficient calculated for motor imagery of the right hand's wrist and fingers are seen in Table 4, Table 5, and Table 6.

In Table 4 the statistics of 5- or 10-fold cross-validation of data filtered between 8 and 30Hz is shown. After 10-fold cross-validation the variance goes down and the bias is better compared to 5-fold cross-validation. The average kappa value is around the same for 5 and 10-fold cross-validation. The values are in the negative range of kappa. It indicates that the observed and expected agreement do not match. A kappa value of -1 is the result of perfect disagreement.

Table 5 shows the values for the online data filtered between 8-30 Hz and with a nearest neighbour Laplacian reference applied. The average kappa values indicate what was already assumed after the ERDS map examination. The maximal kappa value achieved is much higher than the average of all folds, which is indicated by the standard deviation.

Overall, the classification reliability is below zero. The values are in the range of fair disagreement. The expected agreement is not matching the observed agreement. This matches the participants' feedback on the experience during their session. The participants reported to have the feeling that the system mostly worked by chance or mostly one movement imagery seemed to be classified correctly. The standard deviation value indicates that in some cases the classifier had the ability to classify correctly. It implies that there is data in the entire set which lead to better results than given without cross-validation.

Another interesting question is to see whether a small Laplacian or CAR could improve the results. The values for this are shown in Table 5 and Table 6. A comparison of the values in Table 4 and Table 5 shows that the Laplacian filter does not influence the classifier outcome. The same can be noticed in Table 6. This goes along with what was shown by Ramoser et al. [24]. The values are slightly better for some participants, but for others it is the opposite. The recently published literature suggests that the information for decoding the investigated movements are in the low-frequency range.

The standard deviation indicates a broad range. This can be discussed by the influence of the eye movements which could not be inertly rejected. The number of available trials was already low (rejection-rate from 35 to 66%). To overcome this obstacle, the paradigm has to be adjusted in a manner that the motivation and the tiredness level is constant high and respectively low.

All methods used computed kappa values in the range of no agreement. It is noted, that the maximal kappa could be in the range of slight and fair agreement classification, as there are values above 0.4.

4.2 The Dextrus v1.1 – open hand project

By comparing the open-hand-project-3D-printed hand (see Figure 27) with a human hand (see Figure 29 and Figure 28) several differences can be found:

1. First, the palm of the artificial hand is the housing for the motors. It is stiff and not as flexible as a human hand although ligaments are holding the bones together. The human palm has a vaulted structure and is predestines for holding objects more secure.
2. It is obvious that the human hand has most of its muscles not in the hand itself. The main reason for this is the fact that it would get too clumsy like the Dextrus hand demonstrates. Therefor nature put most of the muscles into the forearm and let them steer the hand like a puppeteer does with his puppets: pulling strings (or in this case ligaments).

3. The joints are all made to act like hinge joints, which is as mentioned before anatomically not correct. This gives the Dextrus hand only one degree of freedom in all joints of the II to V finger.
4. As it is shown in Figure 29 and in Figure 28 many ligaments and muscles control the hand for being able to flex and oppose the digits and to perform different other movements. Compared to the Dextrus hand (Figure 27), the robotic hand is simplified in many manners.

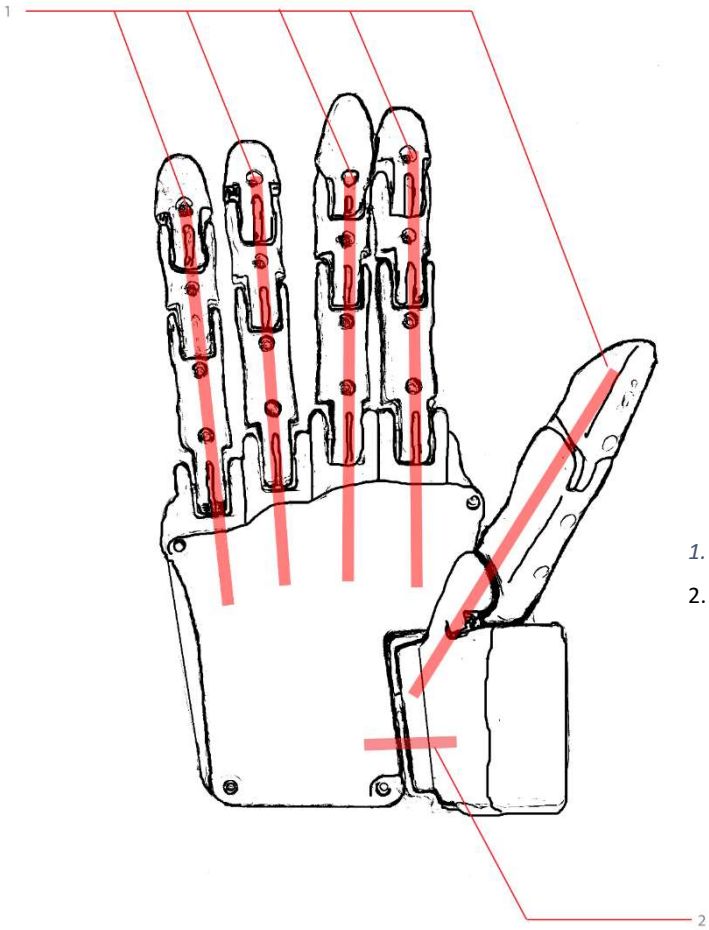

1. *Cable to extend/flex the digits*
2. *Cable for opposition/reposition of the thumb*

Figure 27: "Tendons" of the Dextrus robotic hand (right "hand", frontal view
The "tendons" are a closed loop. Therefore, the counter movement is controlled by the same.

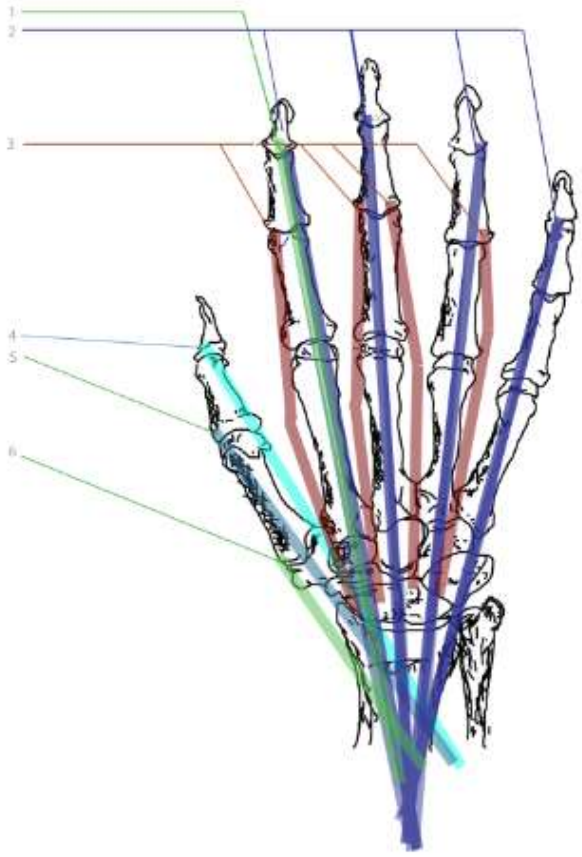

1. *M. extensor indicis*
2. *M. extensor digiti minimi et M. extensor digitorum*
3. *Mm. interossei dorsales*
4. *M. extensor pollicis longus*
5. *M. extensor pollicis brevis*
6. *M. abductor pollicis longus*

Not mentioned: M. extensor carpi radialis logum et brevis und M. extensor carpi ulnaris

Figure 28: Muscles and tendons of the human hand (right hand, dorsal)

The same shows up when comparing Figure 27 and Figure 29. The Dextrus hand is only able to extend and reposition the fingers.

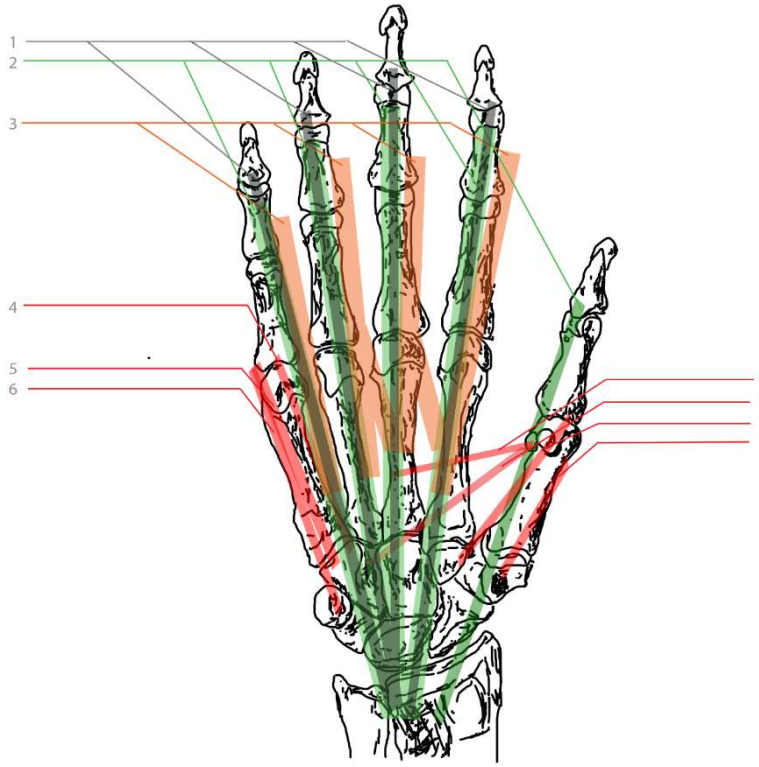

1. *M. flexor digitorum profundus (perforans)*
2. *M. flexor digitorum superficialis (perforatus) et M. flexor pollicis longus*
3. *Mm. lumbricales*
4. *M. flexor digiti minimi brevis*
5. *M. flexor digiti minimi brevis*
6. *M. adductor digiti minimi*
7. *M. adductor pollicis; caput transversum*
8. *M. adductor pollicis; caput obliquuum*
9. *M. flexor pollicis brevis*
10. *M. adductor pollicis brevis et M opponens pollicis*

Not mentioned: M. palmaris brevis

Figure 29: Muscles and tendons of the human hand (right hand, volar)

On the one hand, the comparison shows that many simplifications where done while developing the Dextrus hand. To make flexion and extension possible there is one cable each. This means that the function is not found which the *Mm. lumbricales, Mm. interossei dorsalis,* and *MM adductor* are capable of. Only for the thumb, it is realised. A simplification took place for the functions of the different *Mm. flexor* too. A "one-for-all" flexion is possible. This implies that it is not possible to flex or extend every joint separately, but it is possible to flex every finger on its own. The Dextrus hand uses almost the same functionality to flex the fingers. The human hand has the *M. flexor digitorum superficialis (perforatus) and M. flexor pollicis longus* for this purpose (Comparison with Figure 27 and Figure 29). In comparison with Figure 27 and Figure 28 it is obvious that only the *M. extensor digiti minimi, M. extensor digitorum, and M. extensor pollicis longus* are realised in the Dextrus Hand for extension of the fingers. The third function, the opposition and reposition of the thumb is simulated by copying the functionality of the *M. opponens pollicis* and for the reversed movement the *MM. flexor pollicis longus et brevis*.

On the other hand, it is not possible to extract and classify every movement with EEG (for now?) and the same goes for EMG. This is indicated by the results in this work. The narrower the joints are together, the worse the classification of their movement. Even the movement of the fingers could not be classified precisely against supination and pronation of the hand. Besides that, it would be of benefit if this hand were capable of some other movements, because if there is additional information available for the system then the grasp can be adjusted. One example is grasping a big bottle or a cup. Whereas the former is mostly grasped with slightly abducted fingers, the latter is grasped with adducted fingers. This means that even if the control of the more natural hand movement is not done by the BCI-system, this can be solved by an algorithm and by including supplementary information of the surrounding.

It is questionable if it is necessary to be able to move all fingers individually. When observing most of the grasps performed during the day and comparing the findings of Feix et al. [34] it seems obvious that the index finger and the thumb are solitary moved while the middle finger, ring finger, and pinky are "linked" together by performing the same movement. This means that the control of the artificial hand could be simplified but it would minimize the possibilities too.

Another shortcoming is the lack of feedback from the hand. The only feedback is the current which is needed for the motors. This information is too little because it does not say anything about the position of the fingers. This implies that the hand must be watched while performing. It is also recommended to have a defined starting or ending state, otherwise there is no other way to calibrate the actions to be made.

4.3 The Printed Circuit Board

The PCB could be improved by the use of the L293d Quadruple Half-H Driver [1]. This change would compensate the relays, resistors, diodes, and the transistors. The L293d is able to provide output currents up to 1A at voltages from 4.5V to 36V. As there are four output pins, two motors can be driven in both directions at the same time. As discussed in 4.2, the dynamics of the mostly used grasps would allow to minimize the number of needed drivers to a total of two L293d. The separate control of the artificial hand's fingers would only add one additional driver. The compensation of the driver circuit would reduce the dimension of the PCB resulting in a better handling of the board. The driver IC is designed to diminish electromagnetic interference (EMI). This is another advantage because this eases the designing process of the PCB.

[1] Texas Instruments, L293d Quadruple Half-H Driver, 2016, [ONLINE] Available at: http://www.ti.com/lit/ds/symlink/l293.pdf *[Accessed 23 April 2016]*

5 Conclusion

The aim of this work was to investigate the possibility of controlling an artificial hand with motor imagery. Two classes were selected: Supination and pronation of the right hand and extension and flexion of the right hand's fingers. These movements were indicated by the Dextrus hand's movement of the artificial fingers and the thumb, which compensated the missing possibility to show movements of the wrist respectively of the forearm.

This work states that the classification of movements, whose joints are very narrow to each other is not easy to achieve. Other studies suggest that this information is coded in low frequencies in the range of 0.3 to 3 Hz [42]. The statistics show the barley classification of the imagined movements. The accuracy is beyond or slightly above chance level. The suggested frequency range between 0.3 and 4 Hz could not show any significant change in accuracy of the classifier. With the methods used for this thesis, this frequency range was not applicable. The low kappa values might be explained as follows: The participants attending in the experiments for this thesis were new to the use of BCI systems. For further investigations and getting better results a training session has to be performed to accomplish full awareness over kinaesthetically performed movements. It was reported by every participant that the imagination of these two movements (flexion and extension of the hand's fingers and supination and pronation of the same hand) was hard to get and exhausting. This was noticeable in the raw EEG-data, where the muscle activities and eye-movements and as a result of this also the artefacts increased over time. For the purpose of investigation of the results, about 35% to 66% had to be rejected in the process. Tired participants are a further explanation for the indistinct results. This is noticed when the EOG affected the EEG more often and it cannot be guaranteed that methods, which can rid the EEG of eye movements, remove the influence completely. A longer pause between the runs could help as one participant wished to have more time to relax. Nevertheless, this made the experiment to last even longer and the results did not get better. The problem with eye movement is a potential modulation of brain sources, as it was reported in monkeys [43]. An activation in Brodmann area 44 which was found in experiments with monkeys is not clearly visible in the measured data. The received feedback in form of the bar and especially via the Dextrus robotic hand could also be determined as a source of distraction.

Another point for improvement can be found in the paradigm. The claim for more distinct pauses was reported the most by the users. It was not clear when it will end and how long they have time to swallow and relax. As an improvement it is suggested to add a circular indicator which shows the remaining time for relaxation. The circular shape would minimize the eye movement. The lack of motivation during the experiment could be observed as major disadvantage.

Even this method is intuitive for using a hand, it suffers through the lack of an intuitive response. The visual response by showing the movement by an artificial hand is not natural. The signals from the limb to the brain are not compensated in any way and missing.

The investigation of asynchronous BCI systems would be of high interest and a classification with Fuzzy-Logic, to examine how the results would change.

As previously mentioned additional training is crucial. The movements to perform for this work were reported to be hard to imagine by the subjects. For example, it was stated by the participants, that flexion and extension of the fingers are easier to think about than the movement of the wrist. Keeping all this in mind, the theory proofs that it is a challenging work to do. In 1.2.2 and further in 1.2.2.1 the emergence of EEG and the network needed for signals to result in movements were discussed. The muscles for pronation of the hand are *m. promator teres* (C6-C8 and Th1), *m. pronator quadratus* (C6-C8 and Th1), and *m. brachio radialis* (C5 and C7). The muscles for supination of the hand are *m biceps brachii* (C5-C7), m. supinator (C5-C6) and depending on its state *m. brachio radialis* (C5-C7). The muscles for extension of the fingers are *m. extensor digitorum* (C5-C8 and Th1). The flexion of the fingers is performed by *m. flexor digitorum superficialis* and *profundus* (C5, C7, C8, Th1). Comparing the location of the exit and entry into the spinal nerve, it is obvious that classifying these movements is not easy. The medial nerve is either acting as flexor of the fingers or as pronator. The radial nerve is performing supination and extension of the fingers. This shows that both counter movements are innervated by the same nerve. The flexion is also innervated by the ulnar nerve as shown in Table 1. But the medial nerve gets branches of the truncus inferior as well as the radial nerve does, pointing out that there is also a common source shared with the ulnar nerve which has only branches of this truncus, compared to the others which are fed by different trunci. Figure 3 shows the mapping of the body on the motor cortex. It is visible that the wrist and the fingers are very narrow to each other. It depends on the subject how big these areas are. People who read Braille have a bigger area covered for the index finger [44]. Though, the BCI-system is tested with healthy participants it is not completely sure how well the body parts are represented on the cortex. It might also be thinkable that a person playing the piano has more defined areas because of the need for better control of the fingers. The ability of the development of the cortex is used to regain control over a person's arm, who suffered

partial paralysis after a stroke. This counteracts with the suggestion of intense training of the participants to gain more control and therefore to improve the aptitude for controlling the BCI-system. It will give the opportunity for a subject specific frequency selection and therefor further improvements regarding the accuracy of the BCI-system.

References

[1] H. Berger, „Über das Elektrenkephalogramm des Menschen,“ *Archiv für Psychiatrie und Nervenkrankheiten,* Bd. 87, Nr. 1, pp. 527-570, 1929.

[2] B. Graimann, B. Allison and G. Pfurtscheller, “Brain–Computer Interfaces: A Gentle Introduction,” *Springer-Verlag Berlin Heidelberg,* p. 27, 2010.

[3] S. G. Mason, A. Bashashati, M. Fatourechi, K. F. Navarro and G. Birch, “A Comprehensive Survey of Brain Interface Technology Designs,” *Annals of Biomedical Engineering,* vol. 35, no. 2, p. 137–169, 2007.

[4] A. Y. Paek, Agashe and C.-V. J. L. Harshavardhan A., “Decoding repetitive finger movements with brain activity acquired via non-invasive electroencephalography,” *Frontiers in Neuroengineering,* vol. 7, 2014.

[5] K. Liao, R. Xiao, J. Gonzalez and L. Ding, “Decoding Individual Finger Movements from One Hand,” *PLOS one,* vol. 9, no. 1, 2014.

[6] X. Yong and C. Menon, “EEG Classification of Different Imaginary Movements within the Same Limb,” *PLOS one,* 2015.

[7] G. R. Müller-Putz, R. Scherer, G. Pfurtscheller and C. Neuper, “Temporal coding of brain patterns for direct limb control in humans,” *Frontiers in Neuroscience,* vol. 4, no. 34, pp. 1-11, 2010.

[8] R. Rupp, M. Rohm, M. Schneiders, A. Kreilinger and G. Müller-Putz, “Functional Rehabilitation of the Paralyzed Upper Extremity After Spinal Cord Injury by Noninvasive Hybrid Neuroprostheses,” *Proceedings of the IEEE,* vol. 103, no. 6, pp. 954 - 968, 2015.

[9] F. Binkofski and G. Buccino, “Motor functions of the Broca,” *Brain and Language,* vol. 89, p. 362–369, 2004.

[10] G. Pfurtscheller and C. Neuper, “Motor imagery activates primary sensorimotor area in humans,” *Neurosciencec Letters,* vol. 239, pp. 65-68, 1997.

[11] F. Anderhuber und et.al., „Bewegungsapparat,“ in *Waldeyer Anatomie des Menschen*, Berlin, Walter de Gruyter GmbH & Co. KG, 2012, pp. 218-224.

[12] M. Trepel, Neuroanatomie, München: Elsevier, 2003.

[13] I. Bechman and et.al., “Zentrales Nervensystem, Systema nervosum centrale, Gehirn, Encephalon und Rückenmark, Medulla sinalis,” in *Waldeyer Anatomie des Menschen*, Berlin, Walter de Gruyter GmbH & Co. KG, 2012, pp. 947-1126.

[14] H. H. Jasper, "Report of the committee on methods of clinical examination in electroencephalography: 1957," *Electroencephalography Clinical Neurophysiology,* vol. 10, no. 2, pp. 370-375, 1958.

[15] G. R. Müller-Putz, R. Riedl and S. C. Wriessnegger, “Electroencephalography (EEG) as a Research Tool in the Information Systems Discipline: Foundations, Measurement, and Applications,” *Communications of the Association for Information Systems,* vol. 37, pp. 911-948, 11 2015.

[16] G. Pfurtscheller and A. Aranibar, “Event-related cortical desynchronization detected by power measurements of scalp EEG,” *Electroencephalography and Clinical Neurophysiology,* vol. 42, no. 6, pp. 817-826, 1977.

[17] G. Pfurtscheller and F. Lopes da Silva, “Event-related EEG/MEG synchronization and desynchronization: basic principles,” *Clinical Neurophysiology,* vol. 110, pp. 1842-1857, 1999.

[18] G. Pfurtscheller, C. Neuper, D. Flotzinger and M. Pregenzer, "EEG-based discrimination between imagination of right and left hand movement," *Electroencephalography and clinical Neurophysiology,* vol. 103, pp. 642-651, 1997.

[19] B. He, L. Yang, C. Wilke and H. Yuan, "Electrophysiological Imaging of Brain Activity and Connectivity—Challenges and Opportunities," *IEEE TRANSACTIONS ON BIOMEDICAL ENGINEERING,* vol. 58, no. 7, pp. 1918-1931, 2011.

[20] L. F. Nicolas-Alonso and J. Gomez-Gil, “Brain Computer Interfaces, a Review,” *Sensors,* vol. 12, pp. 1211-1279, 2012.

[21] G. Pfurtscheller, G. R. Müller-Putz, J. Pfurtscheller and R. Rupp, “EEG-Based Asynchronous BCI Controls Functional Electrical Stimulation in a Tetraplegic Patient,” *EURASIP Journal on Applied Signal Processing,* vol. 19, pp. 3152-3155, 2005.

[22] J. R. Wolpaw, N. Birbaumer, D. J. McFarland, G. Pfurtscheller and T. M. Vaughan, “Brain–computer interfaces for communication and control,” *Clinical Neurophysiology,* vol. 113, pp. 767-791, 2001.

[23] M. Tavakolan, X. Xong, X. Zhang and C. Menon, “Classification Scheme for Arm Motor Imagery,” *Journal of Medical and Biological Engineering,* vol. 36, pp. 12-21, 2016.

[24] H. Ramoser, J. Müller-Gerking and G. Pfurtscheller, “Optimal Spatial Filterinf of Single Trial EEG During Imagined Hand Movement,” *IEEE TRANSACTIONS ON REHABILITATION ENGINEERING,* vol. 8, no. 4, pp. 441-446, 2000.

[25] K. Fukunaga, Introduction to Statistical Pattern Recognition, Second Edition, Academic Press, 1990.

[26] Y. Wang, S. Gao and X. Gao, "Common Spatial Pattern Method for Channel Selection in Motor Imagery Based Brain-computer Interface," in *Proceedings of the 2005 IEEE; Engineering in Medicine and Biology 27th Annual Conference*, Shanghai, 2005.

[27] K.-R. Müller, C. W. Anderson and G. E. Burch, “Linear and Nonlinear Methods for Brain-Computer Interfaces,” *IEEE Transactions on Neural Systems and Rehabilitation Engineering,* vol. 11, no. 2, pp. 165-169, 2003.

[28] R. A. Fisher, "TheThe Use of Multiple Measurements in Taxonomic Problems," *Annals of Eugenics,* vol. 7, no. 2, pp. 179-188, 1936.

[29] S. Laszlo, M. Ruiz-Blondet, N. Khalifian, C. Fanny and Z. Jin, “A direct comparison of active and passive amplification electrodes in the same amplifier system,” *Journal of Neuroscience Methods,* vol. 235, p. 298–307, 30 September 2014.

[30] B. Hjorth, “An On-Line Transformation of EEG Scalp Potentials into Orthogonal Source Derivations,” *Electroencephalography and Clinical Neurophysiology,* vol. 39, no. 5, pp. 526-530, 1975.

[31] D. McFarland, “The advantages of the surface Laplacian in brain-computer interface research,” *International Journal of Psychophysiology,* vol. 97, pp. 271-276, 2015.

[32] D. J. McFarland, L. M. McCane, S. V. David and J. R. Wolpaw, “Spatial filter selection for EEG-base communication,” *Electroencephalography and clinical Neurophysiology,* vol. 103, pp. 386-294, 1997.

[33] M. Binder, J. Eitler, J. Deutschmann, S. Ladstätter, F. Glaser and D. Fiedler, “Prosthetics in antiquity—An early medieval wearer of a foot prosthesis (6th century AD) from Hemmaberg/Austria,” *International Journal of Paleopathology,* vol. 12, pp. 29-40, 2016.

[34] T. Feix and J. S. H.-B. D. A. M. Romero, "The GRASP Taxonomy of Human Grasp Types," *IEEE Transactions on Human-Machine Systems,* vol. 46, no. 1, pp. 66-77, 2016.

[35] I. Zein, D. W. Hutmacher, K. C. Tan and S. H. Teoh, “Fused deposition modeling of novel scaffold,” *Biomaterials,* vol. 23, no. 4, pp. 1169-1185, 2002.

[36] T. Hubing, “PCB EMC Design Guidlines: A Brief Annotated List,” in *Electromagnetic Compatibility, 2003 IEEE International Symposium*, 2003.

[37] J. Faller, C. Vidaurre, T. Solis-Escalante, C. Neuper and R. Scherer, "Autocalibration and recurrent adapation: Towards a plug and play online ERD-BCI," *IEEE Transactions on Neural Systems and Rehabilitation Engineering,* vol. 20, no. 3, pp. 313-319, 2012.

[38] J. L. Fleiss, J. Cohen and B. S. Everitt, "Large Sample Standard Errors of Kappa and Weighted Kappa," *Psychological Bulletin,* vol. 72, no. 5, pp. 323-327, 1969.

[39] A. J. Viera and J. M. Garrett, "Understanding Interobserver Agreement: The Kappa Statistic," *Family Medicine,* vol. 37, no. 5, pp. 360-363, 2005.

[40] G. R. Müller-Putz, R. Scherer, C. Brunner, R. Leeb and G. Pfurtscheller, “Better than random? A closer look on BCI results,” *International Journal of Bioelectromagnetism,* vol. 10, no. 1, pp. 52-55, 2008.

[41] K. J. Miller, G. Schalk, E. Fetz, M. de Nijs, J. G. Ojemann and R. P. N. Rao, "Cortical activity during motor execution, motor imagery, and imagery-based online feedback," *Proceedings of he National Academy of Sciences of the United States of America,* vol. 107, no. 9, pp. 4430-4435, 2010.

[42] P. Ofner and G. R. Müller-Putz, "Using a Noninvasive Decoding Method to Classify Rhytmic Movement Imaginations of the Arm in Two Planes," *IEEE Transactions on Biomedical Engineering,* vol. 62, no. 3, pp. 972-980, 2015.

[43] B. Pesaran, M. Nelson and R. Andersen, "Dorsal premotor neurons encode the relative position of the hand, eye, and goal during reach planning," *Neuron,* vol. 51, no. 1, pp. 125-134, 2006.

[44] A. Pascual-Leone and F. Torres, "Plasticity of the sensorimotor cortex representation of the reading finger in Braille readers," *Brain,* vol. 116, no. 1, pp. 39-52, 1993.

Appendix A Printed Circuit Board

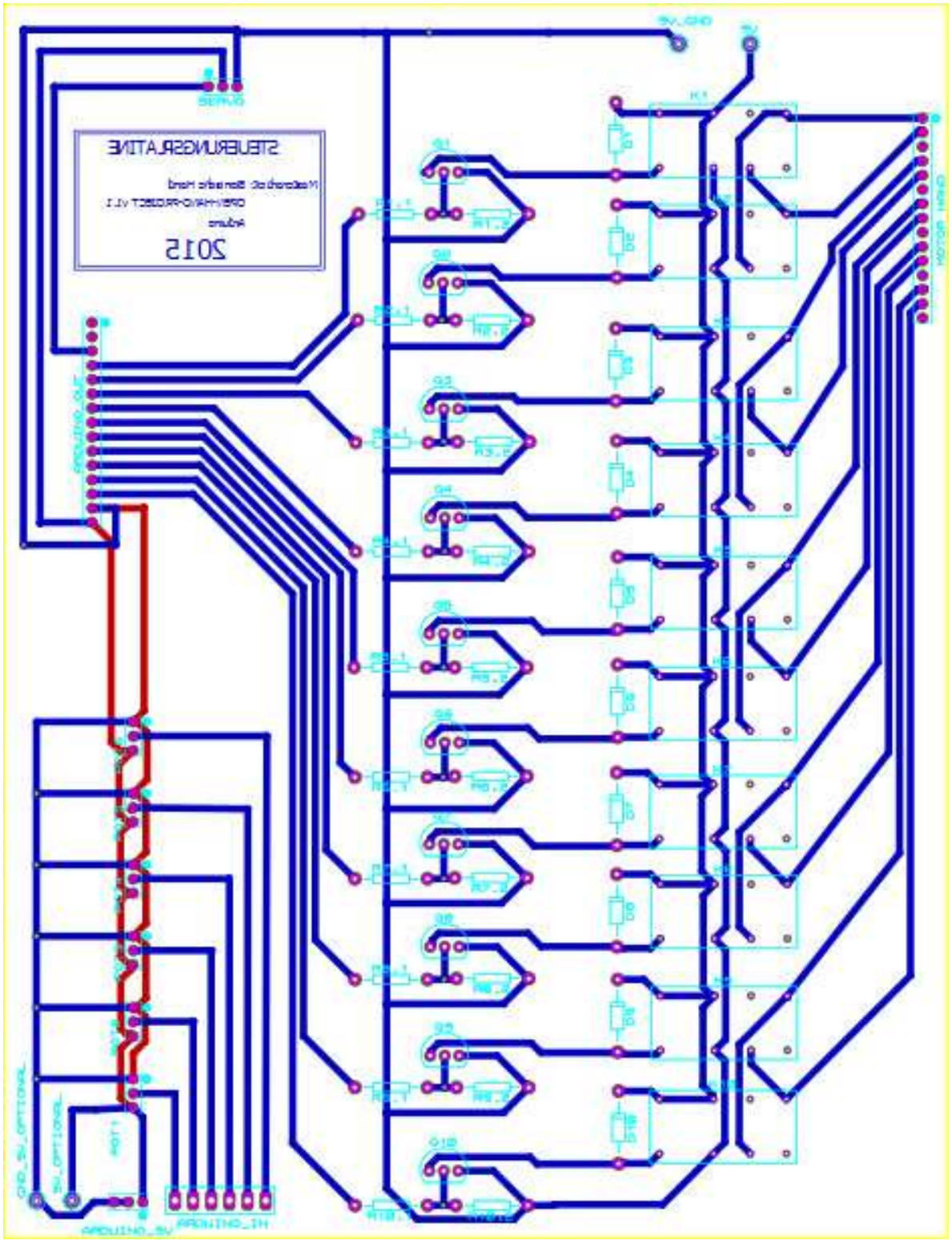

Appendix B Testing script for the PCB and the Dextrus hand

```
// initial servo-object
#include <Servo.h>
Servo myservo;
// constants
// ANALOG IN STATE
const int thumbANALOGPin = A0;
const int thumb2ANALOGPin = A1;
const int indexANALOGPin = A2;
const int middleANALOGPin = A3;
const int ringANALOGPin = A4;
const int pinkyANALOGPin = A5;

// SERVO THUMB
const int thumbServoPin = 2;

// DIGITAL OUT OPEN
const int thumbMotorAPin = 0;
const int indexMotorAPin = 4;
const int middleMotorAPin = 6;
const int ringMotorAPin = 8;
const int pinkyMotorAPin = 10;

// DIGITAL OUT CLOSE
const int thumbMotorZPin = 1;
const int indexMotorZPin = 5;
const int middleMotorZPin = 7;
const int ringMotorZPin = 9;
const int pinkyMotorZPin = 11;

// variables
// <512 equals open; >512 equals closed
int thumbState = 0;
int indexState = 0;
int middleState = 0;
int ringState = 0;
int pinkyState = 0;
int thumbLASTState = 0;
int thumb2LASTState = 0;
int indexLASTState = 0;
int middleLASTState = 0;
int ringLASTState = 0;
int pinkyLASTState = 0;
int pos = 0;
int lowState = 512;

void setup() {
  // put your setup code here, to run once:
  // initialize button pin as input
  pinMode(thumbANALOGPin, INPUT);
  pinMode(thumb2ANALOGPin, INPUT);
  pinMode(indexANALOGPin, INPUT);
  pinMode(middleANALOGPin, INPUT);
  pinMode(ringANALOGPin, INPUT);
  pinMode(pinkyANALOGPin, INPUT);

  // initialize motor output
  pinMode (thumbMotorAPin, OUTPUT);
  pinMode(indexMotorAPin, OUTPUT);
  pinMode(middleMotorAPin, OUTPUT);
  pinMode(ringMotorAPin, OUTPUT);
  pinMode(pinkyMotorAPin, OUTPUT);
  pinMode (thumbMotorZPin, OUTPUT);

  pinMode(indexMotorZPin, OUTPUT);
  pinMode(middleMotorZPin, OUTPUT);
  pinMode(ringMotorZPin, OUTPUT);
  pinMode(pinkyMotorZPin, OUTPUT);

   // attach Servo to pin
  myservo.attach(thumbServoPin);

  // initialize serial communication:
  Serial.begin(9600);
}

void loop() {
  // put your main code here, to run repeatedly:
  // read button states
  thumbState = analogRead(thumbANALOGPin);
  thumbState= map(  thumbState, 0, 1023, 0, 1023);
  indexState = analogRead(indexANALOGPin);
  middleState = analogRead(middleANALOGPin);
  ringState = analogRead(ringANALOGPin);
  pinkyState = analogRead(pinkyANALOGPin);

 pos = analogRead(thumb2ANALOGPin);
// reads the value of the potentiometer (value
between 0 and 1023)
 pos = map(pos, 0, 1023, 0, 179);     // scale it to
use it with the servo (value between 0 and 180)

  if ( (thumbState > lowState) && (thumbState !=
thumbLASTState) && (thumbLASTState >
thumbState)) {
      Serial.println("Daumen AUF");
      digitalWrite(thumbMotorAPin, HIGH);
      thumbLASTState = thumbState;}
    else {
      digitalWrite(thumbMotorAPin, LOW);}

  if ( (thumbState < lowState) && (thumbState !=
thumbLASTState) && (thumbLASTState <
thumbState)) {
      Serial.println("Daumen ZU");
      digitalWrite(thumbMotorZPin, HIGH);
      thumbLASTState = thumbState;}
    else {
      digitalWrite(thumbMotorZPin, LOW);}

  // thumb SERVO
  if (( pos != thumb2LASTState) && (pos >
thumb2LASTState)) {
      Serial.println("Daumen ADduzieren");

      // set new servo position
      myservo.write(pos);
      // wait 15msec
      delay(15);
      thumb2LASTState = pos;
    }

  if (( pos != thumb2LASTState) && (pos <
thumb2LASTState)) {
      Serial.println("Daumen ABduzieren");
      // set new servo position
      myservo.write(pos);
      // wait 15msec
      delay(15);
      thumb2LASTState = pos;
    }
 if ( (indexState > lowState) && (indexState !=
indexLASTState) && (indexLASTState >
indexState)) {
      Serial.println("Daumen AUF");
      digitalWrite(indexMotorAPin, HIGH);
      indexLASTState = indexState;}
    else {
      digitalWrite(indexMotorAPin, LOW);}

  if ( (indexState < lowState) && (indexState !=
indexLASTState) && (indexLASTState <
indexState)) {
      Serial.println("Daumen ZU");
      digitalWrite(indexMotorZPin, HIGH);
      indexLASTState = indexState;}
    else  {
      digitalWrite(indexMotorZPin, LOW);}

  if ( (middleState > lowState) && (middleState !=
middleLASTState) && (middleLASTState >
middleState)) {
      Serial.println("Daumen AUF");
      digitalWrite(middleMotorAPin, HIGH);
      middleLASTState = middleState; }
    else  {
      digitalWrite(middleMotorAPin, LOW);}

  if ( (middleState < lowState) && (middleState !=
middleLASTState) && (middleLASTState <
middleState)) {
      Serial.println("Daumen ZU");
      digitalWrite(middleMotorZPin, HIGH);
      middleLASTState = middleState; }
    else  {
      digitalWrite(middleMotorZPin, LOW);}

  if ( (ringState > lowState) && (ringState !=
ringLASTState) && (ringLASTState > ringState)) {
      Serial.println("Daumen AUF");
      digitalWrite(ringMotorAPin, HIGH);
      ringLASTState = ringState;  }
    else {
      digitalWrite(ringMotorAPin, LOW);}

  if ( (ringState < lowState) && (ringState !=
ringLASTState) && (ringLASTState < ringState)) {
      Serial.println("Daumen ZU");
      digitalWrite(ringMotorZPin, HIGH);
      ringLASTState = ringState;}
    else {
      digitalWrite(ringMotorZPin, LOW);}

  if ( (pinkyState > lowState) && (pinkyState !=
pinkyLASTState) && (pinkyLASTState >
pinkyState)) {
      Serial.println("Daumen AUF");
      digitalWrite(pinkyMotorAPin, HIGH);
      pinkyLASTState = pinkyState;}
    else {
      digitalWrite(pinkyMotorAPin, LOW);}

  if ( (pinkyState < lowState) && (pinkyState !=
pinkyLASTState) && (pinkyLASTState <
pinkyState)) {
      Serial.println("Daumen ZU");
      digitalWrite(pinkyMotorZPin, HIGH);
      pinkyLASTState = pinkyState;}
    else {
      digitalWrite(pinkyMotorZPin, LOW);}
}
```